



Resource

<https://doi.org/10.1038/s44161-022-00138-1>

Spatiotemporal transcriptomics reveals pathogenesis of viral myocarditis

Received: 5 January 2022

Accepted: 25 August 2022

Published online: 10 October 2022

Check for updates

Madhav Mantri ¹, Meleana M. Hinchman ², David W. McKellar ¹, Michael F. Z. Wang ¹, Shaun T. Cross ^{1,2,3}, John S. L. Parker ^{2,3} and Iwijn De Vlaminck ^{1,3}

A significant fraction of sudden death in children and young adults is due to viral myocarditis, an inflammatory disease of the heart. In this study, by using integrated single-cell and spatial transcriptomics, we created a high-resolution, spatially resolved transcriptome map of reovirus-induced myocarditis in neonatal mouse hearts. We assayed hearts collected at three timepoints after infection and studied the temporal, spatial and cellular heterogeneity of host–virus interactions. We further assayed the intestine, the primary site of reovirus infection, to establish a full chronology of molecular events that ultimately lead to myocarditis. We found that inflamed endothelial cells recruit cytotoxic T cells and undergo pyroptosis in the myocarditic tissue. Analyses of spatially restricted gene expression in myocarditic regions and the border zone identified immune-mediated cell-type-specific injury and stress responses. Overall, we observed a complex network of cellular phenotypes and spatially restricted cell–cell interactions associated with reovirus-induced myocarditis in neonatal mice.

Viral infection is the most common cause of myocarditis^{1,2}. The resulting inflammatory cardiomyopathy can lead to arrhythmias, dilated cardiomyopathy and death^{1,3,4}. In humans, viral myocarditis is challenging to study because of the low sensitivity of available diagnostic testing, the acute onset of the disease, the focal nature of the disease and the extreme heterogeneity of immune–virus interactions in complex cardiac tissues^{4–6}. In mice, mammalian orthoreovirus offers a flexible model system⁷. After oral inoculation, the type 1 Lang (T1L) reovirus strain initially infects the gastrointestinal tract. Within days, the infection then spreads to secondary sites in the body, including the heart, leading to myocarditis in up to 50% of infections^{7–9}. However, even in this mouse model, the molecular pathogenesis of viral myocarditis is difficult to study because of the complex network of cardiac and immune cell types involved and the cellular, spatial and temporal heterogeneity of the disease^{2,10}. Consequently, neither the cell types that are responsible for the innate immune response nor the cell types that are infected *in vivo* have been identified. Similarly, the responses of infected and uninfected bystander cells within the heart have not been

characterized. In addition, the protective versus damaging effects of adaptive immune responses have not been quantified. Experiments in mice with severe combined immunodeficiency (SCID) indicate that adaptive immune responses are not required for myocardial injury and heart failure^{7,11}, but these observations do not exclude the possibility that immune-cell-mediated injury is important in immunocompetent mice. Unbiased characterization of all cellular phenotypes as a function of time and location within infected cardiac tissues is needed to address these knowledge gaps.

In this study, we used integrated single-cell and spatially resolved RNA sequencing (RNA-seq) to study the cellular and spatial heterogeneity of myocarditic processes in the hearts of reovirus-infected neonatal mice at multiple timepoints after infection. We also applied these technologies to study the innate response to reovirus infection in the intestine. In addition, we performed time-series single-cell RNA sequencing (scRNA-seq) of cardiac tissues of mice infected with a reovirus point mutant that does not cause myocarditis. To establish viral tropism, we implemented molecular enrichment of non-polyadenylated viral

¹Nancy E. and Peter C. Meinig School of Biomedical Engineering, Cornell University, Ithaca, NY, USA. ²Baker Institute for Animal Health, College of Veterinary Medicine, Cornell University, Ithaca, NY, USA. ³Cornell Institute for Host-Microbe Interactions and Disease, Cornell University, Ithaca, NY, USA.
 e-mail: jsp7@cornell.edu; vlaminck@cornell.edu

transcripts that were otherwise poorly represented in the transcriptomes. Our measurements give insight into the cell type specificity of innate immune responses, into the tropism of the virus in the intestine and the heart and into the transcriptional states of cell types involved in the production of inflammatory cytokines and the recruitment of circulating immune cells. Analyses of spatially restricted gene expression in myocarditic regions and the border zone around those regions identified injury and stress responses in different cell types, including cardiomyocytes. Overall, our data identify spatially restricted cellular interactions and cell-type-specific host responses during reovirus-induced myocarditis.

Spatiotemporal transcriptomics of reovirus-infected hearts

To elucidate the pathogenesis of reovirus-induced myocarditis, we analyzed heart tissues collected from neonatal mice infected orally with either the T1L strain of reovirus or a mock control (Methods and Fig. 1a). We generated scRNA-seq data for 31,684 cells from infected hearts and mock controls at 4, 7, and 10 days post-infection (dpi) and 8,243 spatial transcriptomes for four tissue sections from infected hearts and mock controls at 4 dpi and 7 dpi from the same litter (10x Chromium and 10x Visium; Methods, Extended Data Fig. 1a,b and Fig. 1b,c). The single-cell transcriptomes represented 18 distinct cell types, including cardiomyocytes, endocardial cells, cardiac fibroblasts, endothelial cells, mural cells, macrophages, neutrophils, natural killer (NK) cells, dendritic cells, T cells and B cells (Methods, Fig. 1b, Supplementary Table 1 and Extended Data Fig. 1c–f). Clustering of the spatial transcriptomic data revealed distinct transcriptional programs for myocarditic regions and the border zone surrounding the myocarditic regions in the 7-dpi reovirus-infected heart that corresponded to areas of tissue damage identified by hematoxylin and eosin (H&E) staining (Fig. 1c and Supplementary Fig. 1a,b). The combination of scRNA-seq and spatial transcriptomics allowed us to resolve and visualize cell types and gene expression in a spatial context (Supplementary Fig. 1c). Because the virus first infects the gastrointestinal tract before it spreads to other body sites, including the heart, we also performed scRNA-seq and spatial transcriptomics on ileum. We obtained 7,695 single-cell transcriptomes and 8,027 spatial spot transcriptomes for ileum from mock and infected samples at 1 dpi and 4 dpi (Fig. 1d and Extended Data Fig. 2a–d).

To faithfully identify reovirus transcripts in the ileum and heart, which are not polyadenylated, we performed hybridization-based enrichment of viral fragments captured in the scRNA-seq libraries (Methods and Extended Data Fig. 3a–c). In the ileum, we captured a total of 13,100 unique viral transcripts, with viral load decreasing from 1 dpi to 4 dpi. At 1 dpi, entero-endocrine cells had the highest fraction of infected cells, followed by enterocytes and goblet cells, all of which are present in the gut epithelium. Lymphatic endothelial cells were infected at 4 dpi, suggesting that the virus reaches the bloodstream via lymphatic drainage to allow transmission of the virus to secondary sites in the body, including the heart, as shown before¹² (Fig. 1e and Extended Data Fig. 3d). We captured 2,762 unique viral transcripts from 392 cells in the T1L-infected hearts. The viral load first increased from 4 dpi to 7 dpi and then decreased from 7 dpi to 10 dpi, consistent with viral titer assays performed on whole hearts^{9,13} (Fig. 1e and Extended Data Fig. 3e). Endocardial and endothelial cells were the most frequently infected cell types at 4 dpi, suggesting that endocardial cells lining the ventricular lumen and endothelial cells lining the cardiac vasculature are among the first cells to be infected (Fig. 1e). We detected an increased infection in endothelial cells from 4 dpi to 7 dpi, consistent with viral titer assays performed on whole hearts^{9,13} (Fig. 1e and Extended Data Fig. 3e). We further detected viral transcripts in neutrophils, dendritic cells and T cells in the 7-dpi heart (Fig. 1e and Extended Data Fig. 3e). This observation suggests that antigen-presenting cells and immune cells

may contribute to the spread of infection to other organs in the body. The role of infected dendritic cells in bringing more reovirus to the cardiac tissue during systemic infection has been discussed previously⁸.

To validate these observations, we performed histology, multiplexed RNA fluorescence *in situ* hybridization (FISH) and immunofluorescence assays on tissue sections from myocarditic hearts and controls (multiple infected mice litters; Extended Data Fig. 4a–e and Methods). We used RNA FISH to visualize expression of genes specific to cardiomyocytes, fibroblasts, endothelial cells, macrophages, dendritic cells, neutrophils and T cells (Extended Data Fig. 4c–e, Fig. 1f and Methods). These experiments revealed infection foci and immune infiltration in myocarditic regions. We found *Itgam*⁺*C1qa*⁺ dendritic cells and *Trbc2*⁺ T cells inside the myocarditic regions and *S100a8*⁺ neutrophils in the border zones. In contrast, most *Itgam*⁺*C1qa*⁺ macrophages were found outside the myocarditic regions at 7 dpi (Extended Data Fig. 5c,d). On consecutive tissue sections, we labeled reovirus antigen using immunofluorescence to identify reovirus-infected cells (Extended Data Fig. 4a and Fig. 1f). Co-labelling for the endothelial cell marker *Cdh5* and reovirus transcript M3 on the same tissue sections confirmed the presence of viral transcripts in a subset of cardiac endothelial cells (Extended Data Fig. 4e). Endothelial cells that were positive for the reovirus antigen co-localized with T cells within the myocarditic regions (Fig. 1f). A small number of fibroblasts were often located on the edges of these regions (Fig. 1f). Collectively, these results indicate that vascular endothelial cells are targets of reovirus in the heart.

Endothelial cells initiate host innate immune responses

To detect early transcriptional differences in the cardiac tissue after infection, we performed differential gene expression analysis (DGEA, mock versus infected hearts at 4 dpi; Methods). This analysis revealed a significant upregulation of 230 genes in the infected heart (two-sided Wilcoxon test, log fold change > 1.0 and $P < 0.01$), including genes related to the interferon- β pathway, interferon signaling and innate immune responses (Extended Data Fig. 5a,b and Fig. 2a).

To quantify and compare the overall magnitude of early infection responses across different cell types, we computed a gene module score (infection response (IR) score, module of 230 genes selected above). Comparison of the IR score of different cell types in the absence of infection revealed a small but higher IR score in endothelial cells as compared to other cardiac cell types (Fig. 2b). In response to infection, an increase in IR score was observed for all cardiac cell types, but the greatest increase in IR score was observed for endothelial cells (Fig. 2b). These data suggest that endothelial cells lining the cardiac vasculature are important initiators of the host defense to viral infection. Comparison of IR scores using the spatial transcriptomic data showed increased IR scores in the infected hearts at 4 dpi and 7 dpi, with the highest scores found in myocarditic regions (Fig. 2c). Given our observation that endothelial cells within the heart had the highest IR score in the absence of infection, we asked if this observation was unique to heart tissue or was a more general phenomenon. To this end, we used the Tabula Muris scRNA-seq mouse atlas¹⁴ and estimated the IR score of ~16,000 cells of five major cell types (epithelial cells, fibroblasts, endothelial cells, smooth muscle cells and mesenchymal cells) across ten different organs and tissues. This analysis revealed that endothelial cells consistently had the highest IR score across all tissues in mice (Fig. 2d). These results indicate that endothelial cells lining the vasculature have a higher basal expression of innate response genes within most tissues, which may prime these cells to respond to viral dissemination within the blood and lymphatics.

To investigate the cell-type-specific IR score in the ileum, the primary site of reovirus infection, we performed DGEA on reovirus-infected and mock-infected ileal cells at 1 dpi and found a significant upregulation of 438 genes (two-sided Wilcoxon test, log fold

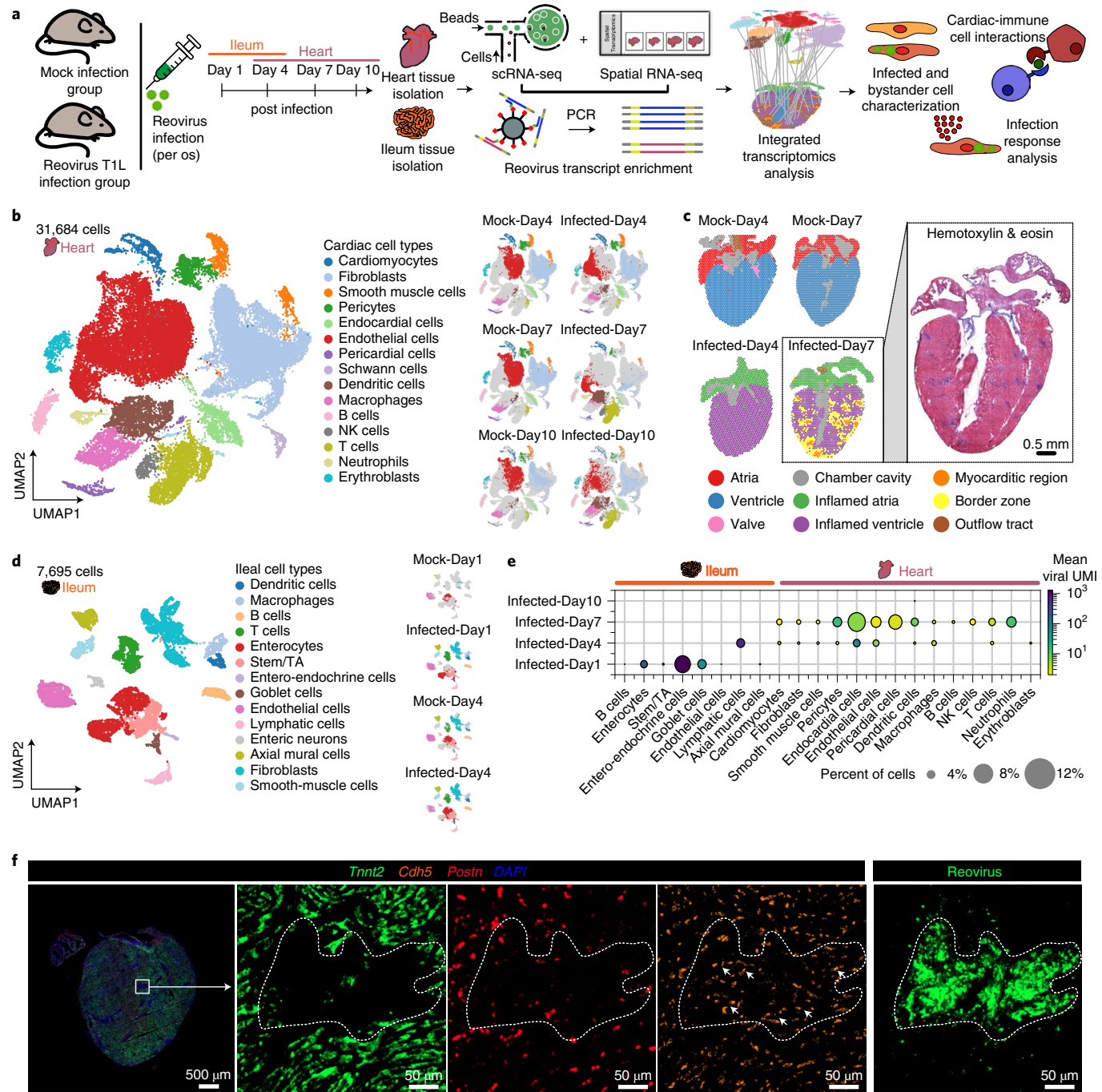


Fig. 1 | Single-cell and spatial transcriptomics of cardiac and ileum tissue of reovirus-infected neonatal mice. **a**, Experiment and analysis workflow. Four-day-old neonatal mice weighing 3 g per pup were infected (per os) with reovirus T1L. Neonatal mice infected with 1× PBS were used as mock controls. Ileum tissue (1 dpi and 4 dpi) and heart tissues (4 dpi, 7 dpi and 10 dpi) were assayed and used for scRNA-seq and spatial transcriptomics. **b**, UMAP plot of 31,684 single-cell transcriptomes from mock-infected and reovirus-infected hearts at 4 dpi, 7 dpi and 10 dpi (one animal per condition), clustered by gene expression and colored by cell type (left). UMAP plots showing cardiac cell type clusters across samples for the heart scRNA-seq data (right). **c**, 8,243 spatial transcriptomes of cardiac tissue sections from mock-infected and reovirus-infected mice at 4 dpi and 7 dpi (one animal per condition). H&E-stained image of reovirus-infected myocarditic

tissue section used for spatial transcriptomics at 7 dpi (in box). **d**, UMAP plot of 7,695 single-cell transcriptomes from mock-infected and reovirus-infected ileum at 1 dpi and 4 dpi, clustered and colored by cell type (left). UMAP plots showing the Gaussian kernel density of cells across samples for the ileum scRNA-seq data (right). **e**, Dot plot showing the percent of cells with non-zero viral transcripts and the mean viral transcript counts (UMIs) in ileal and cardiac cell types. **f**, RNA FISH labeling of cardiac cell type markers (*Trnt2* for cardiomyocytes, *Postn* for fibroblasts and *Cdh5* for endothelial cells) and immunofluorescence staining of reovirus antigen on a consecutive section showing infected endothelial cells within the infection foci at 7 dpi. Representative heart images from six biological replicates.

change > 1.0 and $P < 0.01$), related to the interferon-beta pathway, interferon signaling and innate immune responses in reovirus-infected ileal cells (Extended Data Fig. 5c,d). We computed an IR score using this

module of 438 genes and observed higher basal IR scores in enterocytes and entero-endocrine cells as compared to other ileal cell types (Fig. 2e). Enterocytes further showed the highest increase in IR score

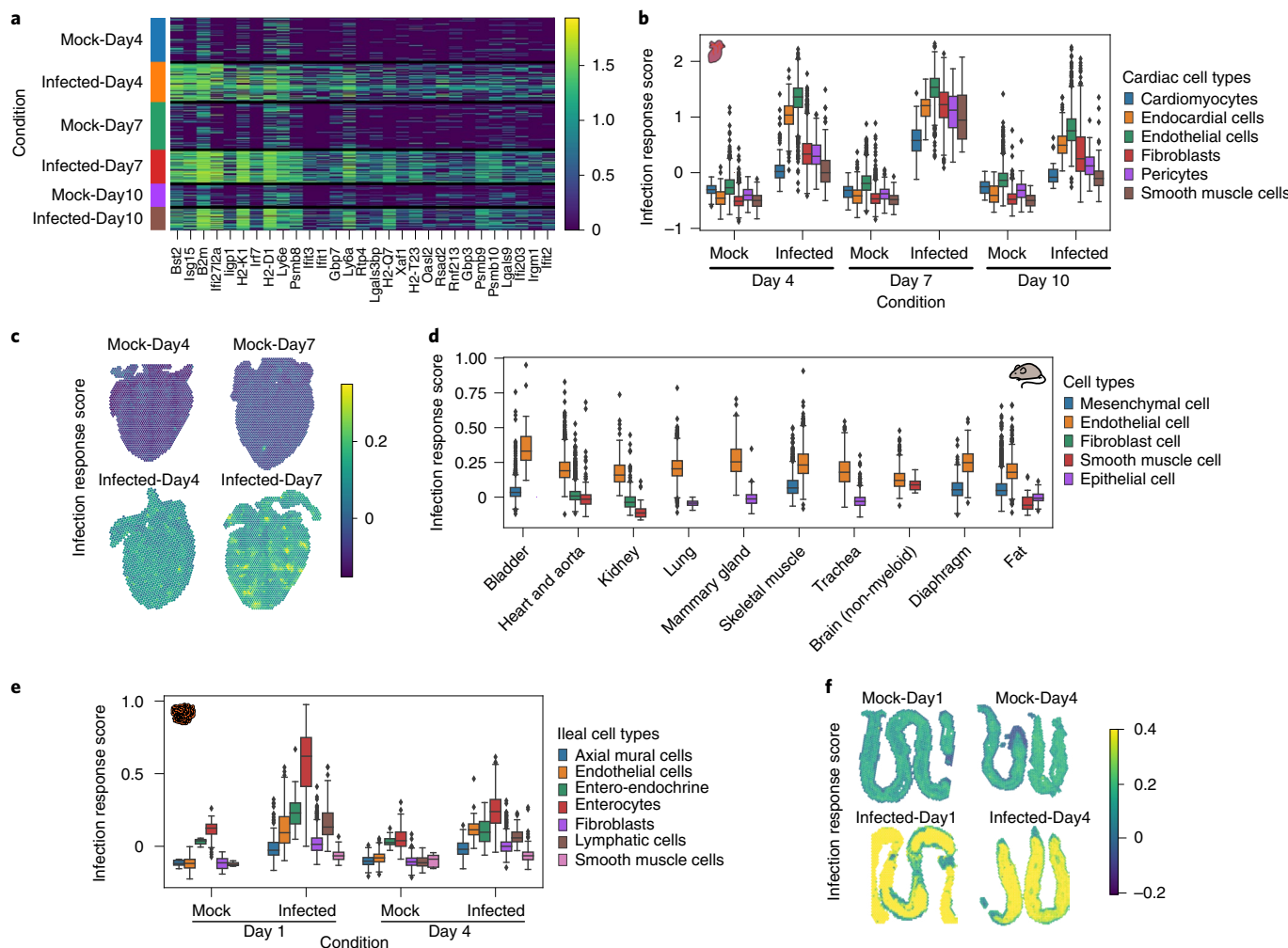


Fig. 2 | Endothelial cells have the highest basal interferon response and the highest increase in innate response upon reovirus infection. **a**, Heat map showing the expression of the 25 most upregulated genes in the reovirus-infected heart as compared to mock at 4 dpi. **b**, Infection response score for cardiac cell types in scRNA-seq data across mock-infected and reovirus-infected hearts at three distinct stages. The infection response score represents the gene module score for a panel of 230 genes that are significantly upregulated (two-sided Wilcoxon test, log fold change > 1.0 and $P < 0.01$) in the reovirus-infected heart as compared to the mock-infected heart at 4 dpi ($n = 23,812$ total cells were examined over six independent experiment conditions; one biologically independent sample was used for each experiment). Boxes in the box plots indicates 25th and 75th percentiles; the band in the box indicates the median; and whiskers extend to $1.5 \times$ IQR of the hinge. Outliers (beyond $1.5 \times$ IQR) are plotted individually. **c**, Infection response score (defined above) across spots in spatial transcriptomics data. **d**, Infection response score calculated for five

after infection, followed by entero-endocrine, endothelial and lymphatic cells (Fig. 2e). Comparison of IR scores for spatial transcriptomic data further supported our analysis of the scRNA-seq data, showing increased IR scores in the infected ileum at 1 dpi and 4 dpi with the highest scores evident within intestinal mucosa and villi (Fig. 2f). The intestinal epithelial cells must tolerate commensal microorganisms present in the lumen of the gut and yet still be responsive to invasive pathogens. Our data suggest that, to achieve this, enterocytes and entero-endocrine cells in the gut epithelium are primed with a basal interferon response and play an important part in mounting innate immune responses in the early stages of viral infection.

common cell types across ten tissues from the Tabula Muris mouse atlas data ($n = 16,651$ total cells were examined over ten independent tissues derived from seven biologically independent animals). **e**, Infection response score for ileal cell types in scRNA-seq data across mock-infected and reovirus-infected ileum at two distinct stages. The infection response score represents the gene module score for a panel of 438 genes significantly upregulated (two-sided Wilcoxon test, log fold change > 1.0 and $P < 0.01$) in the reovirus-infected ileum at 1 dpi as compared to the mock-infected ileum ($n = 5,101$ total cells were examined over four independent experiment conditions; one biologically independent sample was used for each experiment). **d, e**, Boxes in the box plots indicates 25th and 75th percentiles; the band in the box indicates the median; and whiskers extend to 1.5× IQR of the hinge. Outliers (beyond $1.5 \times$ IQR) are plotted individually. **f**, Infection response score for spatial transcriptomics data from mock-infected and reovirus-infected ileum at two distinct stages. IQR, interquartile range.

Endothelial cells recruit T cells and undergo pyroptosis

To explore the heterogeneity of endothelial cell phenotypes in more detail, we reclustered all 9,786 cardiac endothelial cells in the scRNA-seq data. We observed four distinct phenotypes: (1) uninflamed venous endothelial cells expressing *Nr2f2* and *Aplnr* mainly derived from the mock controls¹⁵; (2) arterial endothelial cells expressing *Gja4*, *Gja5* and *Cxcl12* derived from both mock and infected cardiac hearts¹⁵; (3) inflamed endothelial cells derived from infected hearts at 4 dpi and 10 dpi; and (4) inflamed endothelial cells from the heart at 7 dpi, with both inflamed endothelial cell clusters expressing *Isg15*, *lipp1*

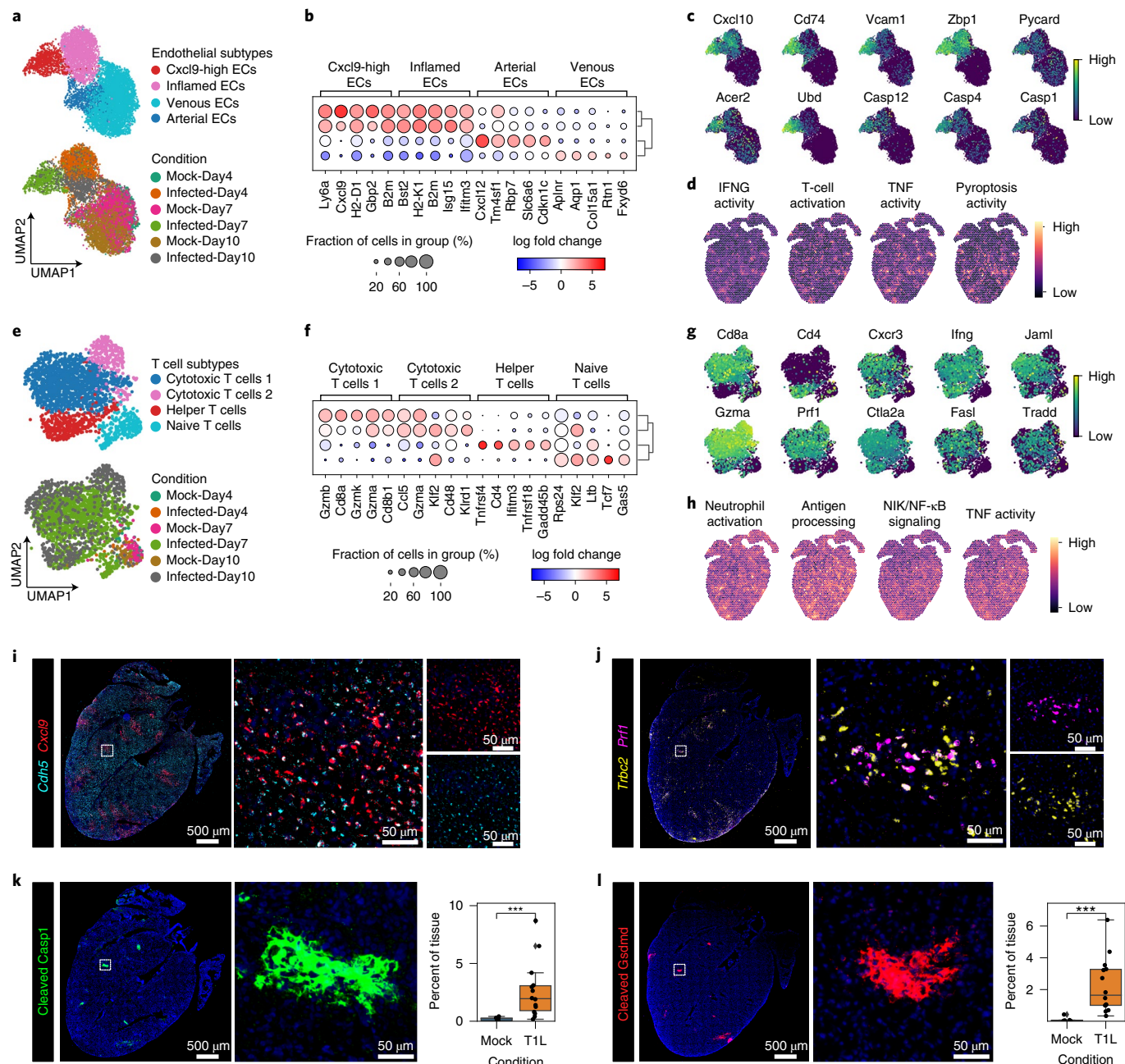


Fig. 3 | Cytotoxic T cells recruited by inflamed endothelial cells induce pyroptosis in myocarditic tissue. **a**, UMAP plot of 9,786 single-cell endothelial cell transcriptomes from mock-infected and reovirus-infected hearts at 4 dpi, 7 dpi and 10 dpi colored by endothelial cell subtype clusters (phenotypes) (top) and condition (bottom). **b**, Heat map showing top five differentially expressed genes (two-sided Wilcoxon test, log fold change > 1.0 and $P < 0.01$) for endothelial cell subtypes. **c**, UMAP plot showing the expression of genes upregulated in Cxcl9-high endothelial cells. **d**, Spatial transcriptomics maps of cardiac tissue from reovirus infected hearts at 7 dpi showing gene module scores calculated for four GO terms enriched in Cxcl9-high endothelial cells. **e**, UMAP plot of 2,205 single-cell T cell transcriptomes from mock-infected and reovirus-infected hearts at 4 dpi, 7 dpi and 10 dpi colored by T cell subtype clusters (top) and condition (bottom). **f**, Heat map showing top five differentially expressed genes (two-sided Wilcoxon test, log fold change > 1.0 and $P < 0.01$) for T cell subtypes. **g**, UMAP plot showing the expression of genes upregulated in cytotoxic T cells from myocarditic heart at 7 dpi. **h**, Spatial transcriptomics maps of cardiac tissue from reovirus infected hearts at 7 dpi

showing gene module scores calculated for four GO terms enriched in cytotoxic T cells. **i,j**, RNA FISH staining for endothelial marker *Cdh5* and chemokine *Cxcl9* (**i**) and T cell marker *Trbc2* and lytic molecule *Prf1* (**j**) on consecutive sections from myocarditic hearts at 7 dpi. Representative images from 14 biological replicates ($n = 7$ males and $n = 7$ females). **k,l**, Immunofluorescence staining for cleaved caspase-1 protein subunit (Casp1 p20 subunit) (**k**) and cleaved gasdermin D protein (GSDMD N terminus fragment) (**l**) on myocarditic hearts at 7 dpi. Representative images from 14 reovirus-infected biological replicates ($n = 7$ males and $n = 7$ females). Immunofluorescence signal from reovirus-infected hearts was compared to mock-infected hearts using two-sided Wilcoxon statistical test. Boxes in the box plots indicates 25th and 75th percentiles; the band in the box indicates the median; and whiskers extend to $1.5 \times$ IQR of the hinge. Outliers (beyond $1.5 \times$ IQR) are plotted individually. P value annotation legend: NS: $P \leq 1.00$; * $1.00 \times 10^{-2} < P \leq 5.00 \times 10^{-2}$; ** $1.00 \times 10^{-3} < P \leq 1.00 \times 10^{-2}$; *** $1.00 \times 10^{-4} < P \leq 1.00 \times 10^{-3}$; **** $P \leq 1.00 \times 10^{-4}$. EC, endothelial cell; IQR, interquartile range; NS, not significant.

and *Ly6a* (Fig. 3a,b). DGEA across endothelial subclusters revealed that the inflamed 7-dpi endothelial cells overexpressed chemokines *Cxcl9* and *Cxcl10*, which are generally involved in immunoregulatory and inflammatory processes but more specifically in the recruitment of T cells and NK T cells¹⁶ (Fig. 3b,c and Extended Data Fig. 6a). In line with this observation, T cells in the 7-dpi hearts expressed the *Cxcr3* receptor (see below). The *Cxcl9*-high inflamed endothelial cells furthermore expressed high levels of cell adhesion marker genes *Vcam1* and *Icam1*, which help immune cells in the blood to attach to endothelial cells¹⁷ (Fig. 3c and Extended Data Fig. 6a,e). The endothelial cells also overexpressed MHC class 1 (*H2-D1* and *H2-K1*) and MHC class 2 (*Cd74*) molecules, suggesting their involvement in antigen presentation to adaptive immune cells (Fig. 3b,c and Extended Data Fig. 6a,e). Endothelial cells have been shown to be involved in antigen presentation and shaping the cellular immune response in infectious myocarditis^{17,18}. Gene Ontology (GO) term enrichment analysis identified pathways further supporting the involvement of *Cxcl9*-high endothelial cells in leukocyte cell–cell adhesion, T cell activation, regulation of interleukin-8 production and response to cytokines, interferon-gamma, interleukin-1 and tumor necrosis factors (Extended Data Fig. 6b).

The observation that endothelial cells are involved in the recruitment of T cells prompted us to explore the heterogeneity of T cells in the infected hearts in more detail. To this end, we reclustered 2,205 T cell single-cell transcriptomes, leading to four subclusters representing three T cell subtypes: (1) *Cd8⁺* cytotoxic T cells, (2) *Cd4⁺* helper T cells and (3) naive T cells (Fig. 3e,f). Both the cytotoxic and helper T cells identified within infected hearts expressed *Cxcr3* receptor, interferon-gamma (*Ifng*) and the chemokines *Ccl3*, *Ccl4*, *Ccl5*, *S100a4* and *S100a6*, suggesting their involvement in neutrophil recruitment and activation (Fig. 3g and Extended Data Fig. 6c). The *Cxcr3* receptor binds selectively to the chemokines *Cxcl9* and *Cxcl10*, promoting chemotaxis (Fig. 3g). Cytotoxic T cells represented most infiltrating T cells and expressed *Prf1*, *Gzma*, *Gzmb* and *Gzmk*, coding for lytic molecules associated with the granzyme-dependent exocytosis pathway¹⁹ (Fig. 3f,g and Extended Data Fig. 6c,g). These cells also expressed tumor necrosis factor superfamily genes *Fasl* and *Tradd*, which are involved in the Fas-induced cell death pathway. *Fasl* binds to *Fas* on the surface of target cells and mediates programmed cell death signaling and NF-κB activation (Fig. 3g). The *Fasl*-*Fas* apoptosis pathway is important in regulating T cells, in promoting tolerance to self-antigens, and is a mechanism by which cytotoxic T cells kill target cells¹⁹. GO term enrichment analysis identified pathways involved in neutrophil activation and degranulation, processing and presentation of exogenous peptide antigen, interleukin-1-mediated signaling pathway, tumor necrosis factor-mediated signaling, NF-κB-inducing kinase (NIK)/NF-κB signaling, cellular response to hypoxia and apoptotic processes (Extended Data Fig. 6d).

The downstream gene markers for cell death-associated pathways *Pycard*, *Acer2*, *Zbp1* and caspases *Casp1*, *Casp4* and *Casp12* were enriched in the *Cxcl9*-high endothelial cells, raising the possibility that cytotoxic lymphocytes are responsible for inflamed endothelial cell death (Fig. 3b,c and Extended Data Fig. 6e). GO term enrichment of endothelial cells confirmed an upregulation of cell death pathways, including activation of cysteine-type endopeptidase activity involved in the apoptotic process, positive regulation of the extrinsic apoptotic signaling pathway and pyroptosis pathway (Extended Data Fig. 6b). We assessed the spatial transcriptomic data to validate direct interactions between *Cxcl9*-high inflamed endothelial cells and T cells and found that they were indeed spatially co-localized in the myocarditic regions and the border zone (Supplementary Fig. 1c). We calculated gene module scores for genes associated with ontology terms enriched in *Cxcl9*-high endothelial and cytotoxic T cells for spatial transcriptomics data and found these pathways to be enriched in the myocarditic regions (Fig. 3d,h, and Extended Data Fig. 6e–h).

We used histology, multiplexed RNA FISH and immunofluorescence to validate our spatial transcriptomic and scRNA-seq findings on

matched tissue sections from myocarditic and mock-infected hearts (Extended Data Fig. 7a,b and Methods). The RNA FISH experiments confirmed the presence of *Cxcl9*-high endothelial cells (detected with *Cdh5*) co-localized with infiltrating T cells within myocarditic tissue (detected by *Trbc2* and lytic molecule *Prf1*; Extended Data Figs. 7a,b and 3i,j). By immunofluorescence microscopy, we found expression of the pyroptosis-mediated cell death marker caspase-1 protein, the active cleaved caspase-1 protein and the pore-forming cleaved gasdermin D protein in myocarditic hearts at 7 dpi (consecutive tissue sections; Extended Data Fig. 7c–e and Fig. 3k,l). These observations support the hypothesis that inflamed endothelial cells undergo pyroptosis in reovirus-infected myocarditic hearts.

Collectively, these results suggest that endothelial cells lining the cardiac vasculature act as a blood–heart barrier and play an important role in the recruitment and activation of the host adaptive immune system. These cells may be the target of both direct viral damage and immune-mediated damage during reovirus-induced myocarditis. Damage to the microvasculature within the heart may then cause loss of blood supply and be a factor in the subsequent death of cardiomyocytes independent of direct viral replication.

Spatially restricted gene expression in myocarditic tissue

The spatially restricted nature of myocarditis motivated us to explore the spatial heterogeneity of gene expression in reovirus-infected hearts. Our initial clustering of the spatial transcriptomic data revealed distinct transcriptional programs for myocarditic regions, the tissue bordering these myocarditic regions and the rest of the ventricular tissue (Figs. 1c and 4a and Supplementary Fig. 1a). Differential spatial gene expression analysis for these regions revealed upregulation in the myocarditic regions of cell type markers for infiltrating immune cells (*Cd8a* and *Gzma* for T cells, *Nkg7* for NK cells and *S100a8* for neutrophils), markers of inflammation (*Cd52* and *Lyc62*; Extended Data Fig. 8a,b) and chemokines and cytokines (*Ccl5*, *Ccl2*, *Cxcl9* and *Cxcl10*). Analysis of the corresponding scRNA-seq data showed that *Ccl5* is expressed by dendritic cells, *Ccl2* by fibroblasts and *Cxcl9* and *Cxcl10* by endothelial cells. The receptor for *Ccl2*–*Ccr2* is expressed in macrophages, indicating that fibroblasts use the *Ccl2*–*Ccr2* axis for macrophage recruitment during myocardial inflammation, as described recently^{20,21} (Extended Data Fig. 8c). Collectively, these analyses suggest that chemokine-producing endothelial cells and cytokine-producing fibroblast cells contribute to the recruitment of immune cells to the myocarditic tissue.

Closer inspection of the myocarditic regions and border zones showed an upregulation of additional genes of interest, including *Tim1*, *AW112010*, *Clu*, *Ankrd1*, *Gm4841* and *Ctss* (Fig. 4B). *Tim1* was mainly expressed by inflamed fibroblasts in the scRNA-seq data (Extended Data Fig. 8d). *Tim1* is a natural inhibitor of the matrix metalloproteinases (MMPs), a group of peptidases involved in the degradation of the extracellular matrix. Upregulation of *Tim1* in patients with deteriorating heart failure was reported previously²². *AW112010* was expressed by inflamed endothelial cells and fibroblasts in the scRNA-seq data. *AW112010* encodes an interferon-induced small secreted protein that regulates inflammation by suppressing IL-10 within pro-inflammatory T-cells²³ (Extended Data Fig. 8d). *Clu* was expressed in a subset of inflamed cells from all cardiac cell types in our data. *Clu* is upregulated during severe myocarditis²⁴ (Extended Data Fig. 8d). *Ctss* was expressed mainly in monocytes (Extended Data Fig. 8d). *Ctss* encodes a protease used for degradation of antigenic proteins to peptides for presentation by MHC class II molecules. Increased formation of immunoproteasomes in susceptible mice has been shown to affect the generation of antigenic peptides and subsequent T cell activity in viral myocarditis^{25,26}. GO term analysis of genes upregulated in the border zone revealed enrichment of terms related to the response to tumor necrosis factor, response to interleukin-1 and NIK/NF-κB signaling (Extended Data Fig. 8e).

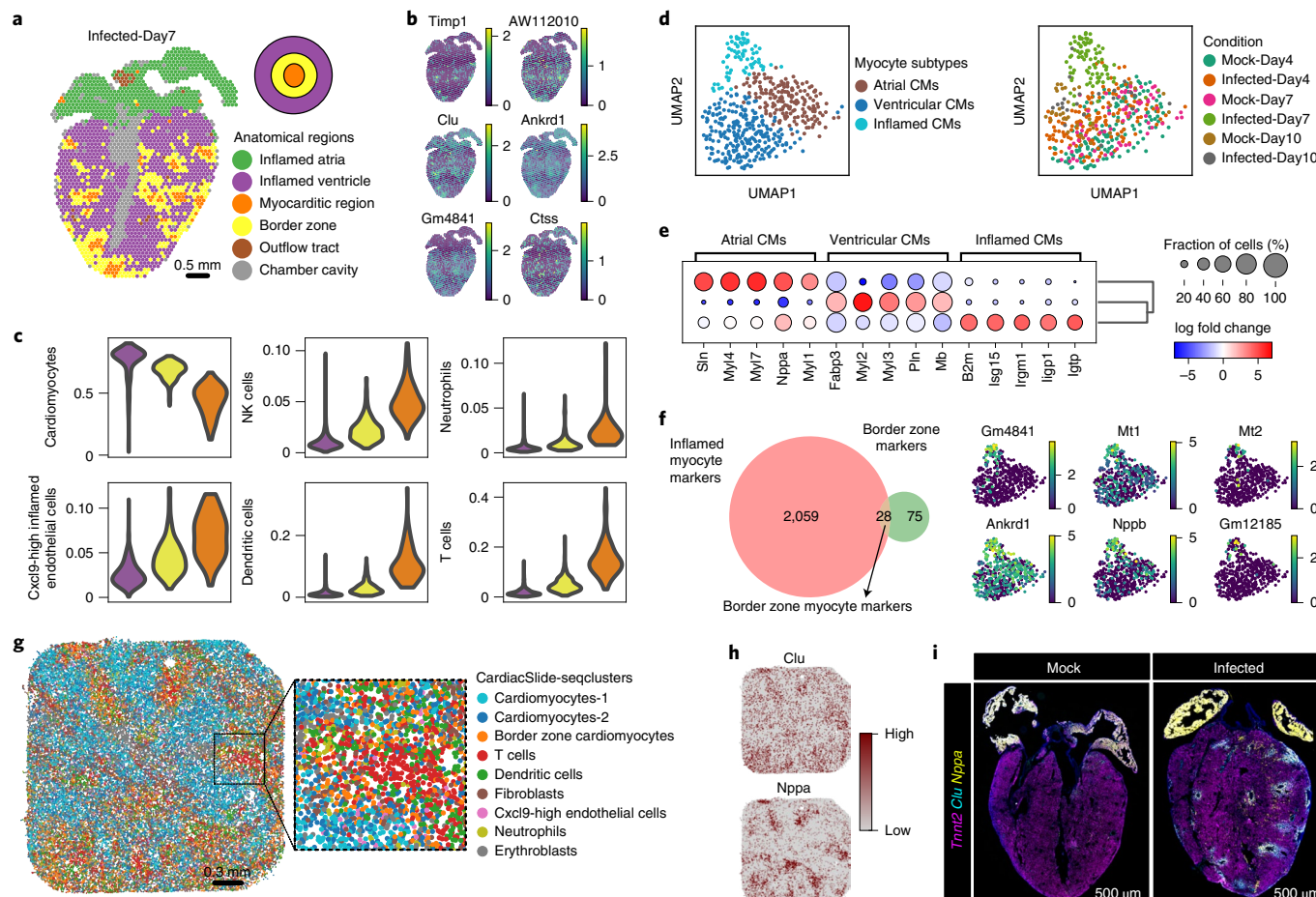


Fig. 4 | Myocarditic regions and the border zone have distinct transcriptomic profiles and cell-type-specific signatures. **a**, Spatial transcriptomics map of cardiac tissue section from reovirus-infected mice at 7 dpi colored by spot clusters representing transcriptionally distinct tissue regions. **b**, Spatial transcriptomics maps of cardiac tissue sections from reovirus-infected mice at 7 dpi showing the expression of differentially expressed genes of interest in the myocarditic and the border zone. **c**, Changes in average predicted cell type proportions across the infected ventricle, for cell types enriched in the myocarditic region and the border zone. **d**, UMAP plot of 502 single-cell cardiomyocyte cell transcriptomes from mock-infected and reovirus-infected hearts at 4 dpi, 7 dpi and 10 dpi colored by myocyte cell subtype (phenotypes) (left) and condition (right). **e**, Heat map showing the top five differentially expressed genes (two-sided Wilcoxon test, log fold change >1.0 and $P < 0.01$) for cardiomyocyte cell subtypes. **f**, Venn diagram showing myocyte-specific genes.

upregulated in the border zone around the myocarditic regions (left), UMAP plot showing the expression of myocyte-specific genes that are upregulated in the border zone of myocarditic regions (right). **g**, High-resolution Slide-seq spatial transcriptomics map of cardiac ventricular tissue from reovirus infected mice at 7 dpi colored by Slide-seq bead clusters. Zoom-in shows the spatial arrangement of Slide-seq clusters within a myocarditic region. **h**, Spatial transcriptomic maps showing Slide-seq expression of four cardiomyocyte-specific genes enriched in inflamed cardiomyocytes as compared to uninflamed myocytes. **i**, RNA FISH staining for cardiomyocyte marker *Tnnt2* and border zone cardiomyocyte markers, such as *Clu* and *Nppa*, on tissue sections from myocarditic hearts and mock controls at 7 dpi. Representative images from 14 reovirus-infected biological replicates ($n = 7$ males and $n = 7$ females) and six mock-infected biological replicates ($n = 3$ males and $n = 3$ females). CM, cardiomyocyte.

To further understand the effect of immune cell infiltration on the cell type composition surrounding the myocarditic regions, we assessed cell type proportions as a function of distance from myocarditic regions in the tissue. We quantified the cell type proportions in myocarditic regions, the border zones and the rest of the ventricular tissue and found that the fraction of *Cxcl9*-high endothelial cells, *Ccl2⁺* fibroblasts, T cells, dendritic cells and NK cells was increased in the myocarditic regions, and the fraction of cardiomyocytes was reduced in myocarditic regions (Fig. 4c and Supplementary Fig. 1c). To understand the phenotype of *Ccl2⁺* fibroblasts enriched in myocarditic region and border zone, we reclustered 9,192 fibroblast cells from the scRNA-seq dataset and identified a distinct cluster of inflamed *Ccl2⁺* fibroblasts from the infected heart at 7 dpi (Extended Data Fig. 8f,g). The *Ccl2⁺* fibroblasts expressed high levels of MHC class I (*H2-D1* and *H2-K1*), adhesion marker genes *Vcam1* and *Icam1* and other genes, such as *Serpina3g*,

C3 and *Ms4a4d* (Extended Data Fig. 8h,i). Moreover, these cells also expressed *Casp1* and *Casp4*, suggesting that fibroblasts also undergo pyroptosis (Extended Data Fig. 8h).

To investigate the effect of inflammation on cardiomyocytes in myocarditic hearts, we reclustered 502 cardiomyocytes from the scRNA-seq dataset and identified three distinct phenotypes: (1) ventricular myocytes expressing *Myl2*, *Myl3* and *Mb* derived from mock and infected hearts at 4 dpi and 10 dpi; (2) atrial myocytes expressing markers *Myl4*, *Myl7* and *Nppa* derived from mock and infected hearts at 4 dpi and 10 dpi; and (3) inflamed myocytes from the infected heart at 7 dpi expressing innate immunity genes *Isg15*, *Igtp* and *Igtp1* (ref. ²⁷) (Fig. 4d,e). Inflamed myocytes from the infected heart at 7 dpi had a distinct phenotype when compared to the myocytes from hearts at 4 dpi and 10 dpi, which clustered with myocyte cells from mock-infected hearts (Fig. 4e). To find transcriptional signatures for myocytes present in the border zone, we selected genes that were both enriched in

cardiomyocytes in the scRNA-seq data and upregulated in the border zone. This analysis revealed that cardiomyocytes in the border zone expressed *Gm4841*, *Gm12185*, *Mt1*, *Mt2*, *Ankrd1* and *Nppb* (Fig. 4f and Extended Data Fig. 8i). *Gm4841* and *Gm12185* are interferon-inducible genes produced in response to interferon-gamma. *Mt1* and *Mt2* genes modulate inflammation and support remodeling in ischemic cardiomyopathy in mice²⁸. Upregulation of *Ankrd1*, a myocyte survival factor, occurs during late-stage heart disease in patients with idiopathic dilated cardiomyopathy²⁹. A recent study shows that cardiomyocytes expressing *Ankrd1* are localized in the border zone on day 1 after myocardial infarction³⁰.

To visualize the spatial distribution and phenotypes of cardiac cell types at higher spatial resolution, we also performed Slide-seq spatial transcriptomics^{31,32} (resolution = 10 μm) on ventricular tissue from a single reovirus-infected myocarditic heart (Methods and Extended Data Fig. 9a). We performed unsupervised clustering and DGEA to label these near single-cell resolution Slide-seq spatial transcriptomes as cardiac cell types (Extended Data Fig. 9b,c and Fig. 4g). We visualized the cell types on the spatial maps and performed neighborhood enrichment analysis, and we observed neutrophils, *Cxcl9*-expressing endothelial cells and border zone cardiomyocytes organized in close proximity to infiltrating T cells and dendritic cells in the myocarditic regions (Extended Data Fig. 9d,e). We furthermore used deconvolution using the scRNaseq data as a reference to obtain cell type predictions and to quantify cell-type-specific gene expression at every spatial location (Methods and Supplementary Fig. 2). We compared the phenotypes of border zone cardiomyocytes and cardiomyocyte-1 clusters using DGEA and confirmed the upregulation of *Ankrd1*, *Nppb*, *Gm4241* and *Saa3*. We furthermore identified additional inflammation and stress-related markers for border zone cardiomyocytes, such as *Clu*³³ and *Nppa*^{34,35} (Extended Data Fig. 9f,g and Fig. 4h,i). We used multiplexed RNA FISH to validate the spatially restricted expression of *Clu* and *Nppa* in cardiomyocytes present in the border zone in reovirus-infected hearts (Fig. 4i and Methods). Together, our analysis reveals that tissue injury is localized to myocarditic regions with remodeling and stress programs being active in the border zone and demonstrates the importance of spatially resolved molecular measurements to study viral myocarditis.

Reduced T cell response associated with K287T mutant

We recently reported a reovirus mutant T1L S4-K287T (K287T) that has a point mutation in the S4 gene encoding outer capsid protein sigma-3 (σ3), a double-stranded (ds) RNA-binding multifunctional protein that promotes viral protein synthesis and facilitates viral entry and assembly⁹. This mutation abolishes the capacity of σ3 to block dsRNA-mediated activation of protein kinase R (PKR). The T1L K287T mutant is less virulent than the wild-type (WT) strain in neonatal mice. K287T replicates to WT titers in the heart at 4 dpi but to significantly lower viral titers than WT virus at 7 dpi. The K287T mutant does not induce myocarditis as observed by calcium staining in the tissue⁹. To confirm our findings about immune-mediated pathogenesis during reovirus infection, we performed additional scRNA-seq for K287T infected hearts at 4 dpi, 7 dpi and 10 dpi. We generated a total of 16,771 single-cell transcriptomes and integrated the data with the data from the WT virus. We did not observe sample-specific clusters after data integration, suggesting minimal experimental batch effects (Fig. 5a and Extended Data Fig. 10a). We performed viral transcript enrichment and compared the mean viral transcripts in WT-infected and mutant-infected cells. We found similar levels of mean viral transcripts for WT and K287T viruses at 4 dpi but a 60-fold lower viral load for K287T at 7 dpi, consistent with viral titer assays⁹ (Extended Data Fig. 10b–e). We then compared the early cardiac cell type host responses to K287T and WT infection. K287T induced a similar level of innate immune responses as WT virus, with endothelial

cells showing the highest increase in cardiac IR score (as defined before) at 4 dpi (Fig. 5b).

We analyzed the cell type composition of inflamed *Cxcl9*-high endothelial cells and immune cells detected in K287T-infected and WT-infected hearts. We observed fewer *Cxcl9*-high endothelial cells and immune cells, including cytotoxic T cells, infiltrating the heart at 7 dpi compared to WT-infected heart (Fig. 5c). These differences correlate with the reduced levels of inflammation associated with the K287T mutant (Fig. 5e). To validate these observations, we performed RNA FISH and immunofluorescence staining on K287T-infected hearts and compared them to mock-infected and reovirus WT-infected hearts (Fig. 5d–h). Immunostaining for reoviral antigen in tissue sections confirmed both a significantly reduced area with viral replication (two-sided Mann–Whitney test, $P < 0.05$) and significantly lower viral antigen within those areas (two-sided Mann–Whitney test, $P < 0.05$), consistent with the scRNA-seq analysis and viral titer assays (Extended Data Fig. 10c and Fig. 5d). We observed a reduction in infiltration of T cells in K287T-infected hearts as compared to WT-infected hearts at 7 dpi (Fig. 5f). The fraction of total cytotoxic immune cells (*Prf1*⁺) was significantly reduced in K287T-infected hearts as compared to WT-infected hearts (two-sided Mann–Whitney test, $P < 0.05$; Fig. 5f). These findings support the reduced immune-mediated cytotoxicity seen in K287T-infected hearts. This was further supported by a significant reduction in cleaved caspase-1 and cleaved gasdermin D protein expression in K287T-infected hearts as compared to WT-infected hearts (two-sided Mann–Whitney test, $P < 1.00 \times 10^{-3}$; Fig. 5g,h). Our results show that cardiac endothelial cells mount a potent and robust innate immune response when infected with the K287T mutant virus. Clearance of the K287T virus from most infected cells by 7 dpi leads to a lower immune-mediated cytotoxicity, which correlates with lack of cardiac injury. These results suggest that a robust early innate immune response in endothelial cells is critical for early viral clearance and prevention of subsequent cardiac injury mediated by cytotoxic immune cells during reovirus-induced myocarditis.

Discussion

Viral myocarditis has been recognized as a cause of heart failure for more than 50 years, but it is still a challenging disease to study, diagnose and treat³⁶. In this study, we used integrated spatial and single-cell RNA-seq to dissect the temporal, spatial and cellular heterogeneity of reovirus-induced acute myocarditis in a neonatal mouse model. We assayed ileum and heart tissues at multiple timepoints after infection. We investigated the cell types that are infected and the cellular and spatial heterogeneity of innate and adaptive immune responses. We generated a total of 13 scRNA-seq and eight spatial transcriptomics datasets, spanning two organs, four timepoints and three infection conditions. Our data provide detailed insight into the chronology of molecular events that lead to reovirus-induced myocarditis. After oral inoculation, reovirus T1L infects entero-endocrine and enterocyte cells in the gut epithelium within 1 dpi. These cells mount a potent innate immune response to inhibit viral replication. The virus then infects the gut lymphatic cells within 4 dpi and is transmitted via lymphatics to the bloodstream and then to secondary sites in the body, including the heart. Around 4 dpi, the virus infects the endothelial cells lining the cardiac vasculature. Endothelial cells mount a potent innate immune response in the heart. In symptomatic cases, inflamed endothelial cells secrete chemokines that recruit circulating immune cells, including cytotoxic T cells. These inflamed endothelial cells then undergo pyroptotic cell death in the myocarditic tissue. Overall, our experiments reveal a dynamic and spatially heterogeneous network of cellular phenotypes and cell–cell interactions associated with reovirus-induced myocarditis.

Integrated high-throughput scRNA-seq and spatial transcriptomics was recently used to study heart development^{37,38} and heart disease^{30,39}, but, to our knowledge, these methods have not been used

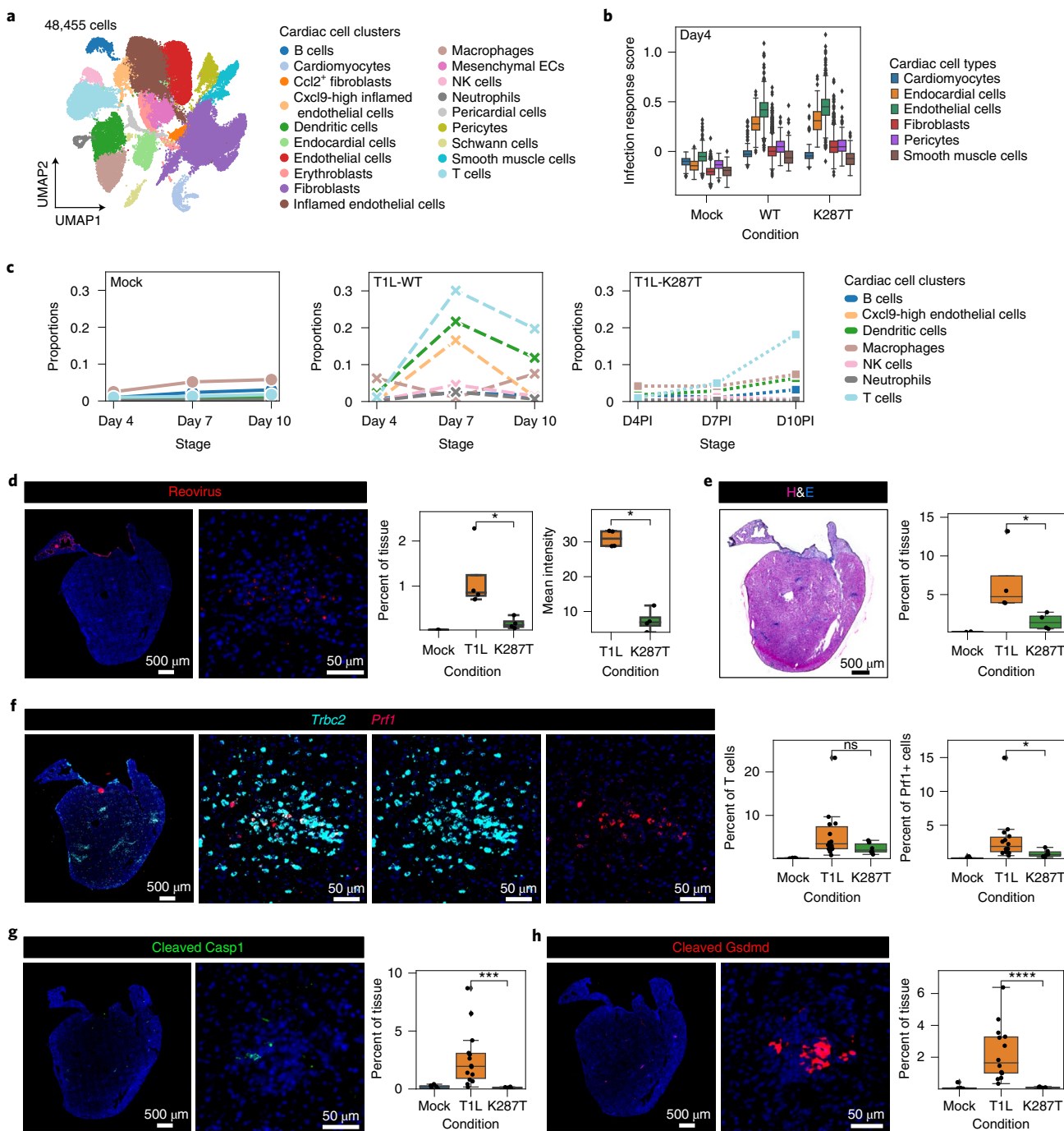


Fig. 5 | A robust innate immune response but reduced adaptive immune cell infiltration explains the non-myocarditic phenotype on infection with reovirus K287T mutant. **a**, UMAP plot of 48,455 single-cell cell transcriptomes from mock-infected, reovirus WT-infected and reovirus mutant (K287T)-infected hearts at 4 dpi, 7 dpi and 10 dpi (one animal per condition) colored by cell type clusters. **b**, Infection response score for cardiac cell types in scRNA-seq data across mock-infected, reovirus WT-infected and reovirus K287T-infected hearts on 4 dpi. The IR score represents the gene module score for a panel of 230 genes that are significantly upregulated (two-sided Wilcoxon test, log fold change > 1.0 and $P < 0.01$) in the reovirus WT-infected sample as compared to the mock-infected sample at 4 dpi ($n = 15$, 510 total cells were examined over nine independent experiment conditions; one biologically independent sample was used for each experiment). Boxes in the box plots indicate 25th and 75th percentiles; the band in the box indicates the median; and whiskers extend to 1.5× IQR of the hinge. Outliers (beyond 1.5× IQR) are plotted individually. **c**, Changes in cell type proportions with time for cell types detected in the myocarditic regions. Panels show the changes in cell type proportions across mock-infected, T1L-WT, and T1L-K287T conditions. **d–f**, Representative heart images from six K287T-infected hearts. **g–h**, Immunofluorescence staining for cleaved caspase-1 protein subunit (Casp1 p20 subunit) (**g**) and cleaved gasdermin D protein (GSDMD N terminus fragment) (**h**) on K287T-infected heart tissue section at 7 dpi. Representative images from six K287T-infected biological replicates ($n = 3$ males and $n = 3$ females). Immunofluorescence signal from K287T-infected hearts was compared to WT-infected hearts using two-sided Wilcoxon statistical test. **d–h**, Boxes in the box plots indicate 25th and 75th percentiles; the band in the box indicates the median; and whiskers extend to 1.5× IQR of the hinge. Outliers (beyond 1.5× IQR) are plotted individually. P value annotation legend: NS: $P \geq 0.05$; * $P < 0.05$; ** $P < 0.01$; *** $P < 0.001$; **** $P < 0.0001$. IQR, interquartile range; NS, not significant.

reovirus WT-infected and reovirus K287T-infected cells. **d**, Immunofluorescence images of reovirus antigen on reovirus mutant (K287T)-infected hearts at 7 dpi. **e**, H&E-stained image of K287T-infected heart tissue section at 7 dpi. **f**, RNA FISH staining for T cell marker *Trbc2* and lytic molecule *Prf1* on K287T-infected heart tissue section at 7 dpi. **d–f**, Representative heart images from six K287T-infected hearts. **g–h**, Immunofluorescence staining for cleaved caspase-1 protein subunit (Casp1 p20 subunit) (**g**) and cleaved gasdermin D protein (GSDMD N terminus fragment) (**h**) on K287T-infected heart tissue section at 7 dpi. Representative images from six K287T-infected biological replicates ($n = 3$ males and $n = 3$ females). Immunofluorescence signal from K287T-infected hearts was compared to WT-infected hearts using two-sided Wilcoxon statistical test. **d–h**, Boxes in the box plots indicate 25th and 75th percentiles; the band in the box indicates the median; and whiskers extend to 1.5× IQR of the hinge. Outliers (beyond 1.5× IQR) are plotted individually. P value annotation legend: NS: $P \geq 0.05$; * $P < 0.05$; ** $P < 0.01$; *** $P < 0.001$; **** $P < 0.0001$. IQR, interquartile range; NS, not significant.

to study viral myocarditis before our work. Bulk RNA-seq has been used previously to profile transcriptomic signatures of infection, inflammation and tissue injury associated with viral myocarditis^{9,40–43}. However, these ensemble-level approaches do not capture the cellular and spatial heterogeneity of host response to infection. scRNA-seq has recently been used to study coxsackievirus B3 (CVB3)-induced myocarditis in a mouse model⁴⁴. Lasrado et al. reported inflammatory phenotypes of myeloid cells, the role of fibroblasts in remodeling and inflammation and the role of cytotoxic T cells in CVB3-induced myocarditis. However, the cardiac cell types that are targeted by the virus, the cell type heterogeneity in basal interferon response and innate immune response and the spatial restriction of transcriptional programs were not explored in this study⁴⁴.

Reovirus infection occurs often in humans, but most cases are mild or subclinical. These viruses display a broad host range, but only young hosts develop the disease. After infection of neonatal mice, reoviruses cause injury to a variety of organs, including the heart, liver and the central nervous system, depending on the viral strain. Reovirus T1L strain is mildly virulent and causes myocarditis in ~50% of the infected mice. Neonatal mice with myocarditic hearts due to T1L infection survive with tissue damage and have an increased rate of heart failure. Therefore, reovirus T1L infection in neonatal mice is an ideal model to study the mechanisms and pathogenesis of reovirus-induced myocarditis in young hosts. Previous studies have claimed that the direct cytopathic effect of viral replication on cardiac cells is the main cause of cardiac damage during reovirus-induced myocarditis^{7,45}. Notably, Sherry et al. found that reovirus infection can induce myocarditis in immunodeficient mice lacking B and/or T cells, suggesting that reovirus-induced myocarditis does not strictly require adaptive immunity^{7,41}. However, these previous experiments do not rule out the possibility that the host adaptive immune response can augment or delimit the nature and amount of host damage in immune-competent mice, as is suggested by our work. In addition, the viral strain used in these experiments was substantially more virulent. Holm et al. and Stewart et al. studied the protective role of innate immune responses in reovirus-induced myocarditis^{13,46}. However, before our study, the temporal, spatial and cell type heterogeneity of basal type-I IFN and innate immune responses to infection had not, to our knowledge, been characterized. Miyamoto et al. and Stewart et al. compared basal levels of type-I IFN between cardiac myocytes and fibroblasts *in vitro*, but these studies did not include all the cell types that make up complex cardiac tissues^{27,47}.

Spatiotemporal characterization of viral myocarditis is crucial to understanding the viral and host factors that are important for disease pathology. This knowledge may ultimately lead to novel diagnostic approaches and better treatments. Several viruses that frequently infect humans can cause myocarditis, including adenovirus, enteroviruses, Epstein–Barr virus, human herpesvirus 6, parvovirus B19 and severe acute respiratory syndrome coronavirus 2 (SARS-CoV-2). The results presented here may not be representative of the mechanisms for other viral causes of myocarditis or viral myocarditis in adult hosts. However, the approaches that we have implemented here can be used in future studies to investigate how the induction, pathophysiology and course of myocarditis induced by these viruses differs. We hope that the data and analysis routines that we make available here will be a valuable resource for such future studies.

Methods

Ethical approval for animal experiments

All animal work was conducted ethically, conforming to the US Public Health Service policy, and was approved by the Institutional Animal Care and Use Committee at Cornell University (IACUC no. 2019-0129). Confirmed pregnant female C57BL/6J mice were ordered from Jackson Laboratories to be delivered at embryonic stage E14.5. Mice were housed in 11.5-inch × 7.5-inch IVC Polycarb Shoebox Cages for the duration of the experiment. Temperature 68–77 °F and humidity between

30% and 70% were maintained in the rodent room. Lights were turned on at 5:00 and off at 19:00 in the rodent room.

Reovirus infections of neonatal C57BL/6J mice

Litters weighing 3 g per pup were gavaged using intramedic tubing (Becton Dickinson, 427401) per os with 50 µl with 10⁷ plaque-forming units (PFU) of reovirus T1L:WT or K287T mutant in 1× PBS containing green food color (McCormick) via a 1-ml tuberculin slip tip syringe (BD, 309659) and a 30-gauge × 1/2 needle (BD, 305106). Litters treated with 1× PBS containing green food color alone on the same day were used as mock controls for the respective infection groups. The mock-infected and reovirus-infected mice pups were weighed daily until the timepoints used in the study (1, 4, 7 and 10 dpi). Due to the difficulty in determining the sex of mice during infection and early neonatal stages, we randomly selected the mice to collect ileum and heart tissues for scRNAseq and spatial transcriptomics experiments (Supplementary Table 2).

Sample preparation for single-cell transcriptomics of cardiac tissue

We sacrificed mock-infected and reovirus-infected C57BL/6J mice on 4 dpi, 7 dpi and 10 dpi and collected cardiac tissues for single-cell transcriptomics. Single heart tissue from respective stages (one heart per stage) was isolated aseptically, washed with ice-cold HBSS (with calcium and magnesium chloride; Gibco, 14025-134) and minced into 1–2-mm pieces. Cardiac tissue pieces were then digested in tissue dissociation media with 200 U ml⁻¹ of collagenase type II (Gibco, 17100-015), 1 mg ml⁻¹ of dispase (Sigma-Aldrich, D4693) and 3 mM calcium chloride in HBSS for four cycles of 10 minutes under mild agitation at 37 °C in 1.5-ml Eppendorf tubes. After every 10-minute cycle, cell suspension was collected, added to ice-cold 1× PBS with 0.04% BSA (Sigma-Aldrich, A3803), and new dissociation media was added to the tubes. At the end of the digestion, the cells were passed through a 70-µm filter and centrifuged into a pellet. To remove most blood contaminants, samples were resuspended in an ammonium-chloride-potassium (ACK) lysis buffer (Lonza, 10-548E) for 3–5 minutes and centrifuged. Samples were then washed again in PBS with 0.04% BSA and then resuspended at 1 × 10⁶ cells per milliliter. Cells from each sample were stained with trypan blue, and cell viability was calculated on an automated cell counter (Countess II) before loading the cells on 10x Chromium. We used these cell viabilities to adjust the number of cells loaded on 10x Chromium to get the desired number of transcriptomes from viable cells for each sample (5,000 cells per sample).

Sample preparation for single-cell transcriptomics of intestinal tissue

We sacrificed mock-infected and reovirus-infected C57BL/6J mice on 1 dpi and 4 dpi and collected intestinal ileum tissue for single-cell transcriptomics. Single intestinal ileum tissue from respective stages (one tissue per stage) was isolated aseptically and washed with ice-cold HBSS (without calcium and magnesium chloride; Gibco, 14175-095) to remove contamination. The ileum tissue was then opened longitudinally, washed again with HBSS and minced into 1–2-mm pieces. To isolate the epithelial layer of cells, ileum tissue pieces were incubated in HBSS with 10 mM EDTA (Invitrogen, 15575-038) and 1 mM DTT (Sigma-Aldrich, 43816-10ML) for two cycles of 10 minutes under mild agitation at 37 °C. After every 10-minute cycle, cell suspension containing the intestinal epithelial cells was collected and added to ice-cold 1× PBS with 0.04% BSA (Sigma-Aldrich, A3803). The undigested pieces of lamina propria were then washed thoroughly with PBS (with calcium and magnesium chloride; Gibco, 14080-055) to get rid of all EDTA. These pieces were then transferred to fresh tubes and incubated in 200 U ml⁻¹ of collagenase type I (Gibco, 17100-017) and 3 mM calcium chloride in PBS for three cycles of 10 minutes under mild agitation at 37 °C in 1.5-ml Eppendorf tubes. After every 10-minute cycle, cell suspension containing the lamina propria cells was collected and added to ice-cold PBS with 0.04% BSA in separate tubes. At the end of the digestion, the cells were passed

through a 40- μm filter and washed twice in PBS with 0.04% BSA and then resuspended at 1×10^6 cells per milliliter. Cells from intestinal epithelium and lamina propria for each sample were stained with trypan blue, and cell viability was calculated on automated cell counters (Countess II). Cell counts adjusted with viability were then pooled as 40% epithelial cells and 60% lamina propria to adjust the number of cells loaded on 10x Chromium and to get the desired number of transcriptomes from viable cells for each sample (5,000 cells per sample).

scRNA-seq library preparation

In total, 5,000–6,000 viable cells per sample (for heart and ileum tissues) were targeted on the Chromium platform (10x Genomics) using one lane per sample per timepoint. Single-cell libraries were built using the Chromium Next GEM Single Cell 3' Library Construction V3 Kit (10x Genomics) and were then sequenced on an Illumina NextSeq 500 using 75-cycle high-output kits (Index 1 = 8, Read 1 = 28 and Read 2 = 55) for all samples. Sequencing data were aligned to a combined mouse and reovirus reference genome (described below) using the Cell Ranger 6.0.0 pipeline (10x Genomics).

Hybridization-based enrichment of viral fragments

We performed a hybridization-based enrichment of viral fragments on a part of scRNA-seq libraries using xGen NGS target enrichment kit (Integrated DNA Technologies, 1080577). In this approach, a panel of 5'-biotinylated oligonucleotides is used for capture and pulldown of target molecules of interest, which are then PCR amplified and sequenced. We designed a panel of 202 biotinylated probes tiled across the entire reovirus T1L genome to selectively sequence viral molecules from the scRNA-seq libraries (Supplementary Table 3). Then, 300 ng of fragmented and indexed scRNA-seq libraries from reovirus WT-infected hearts, reovirus mutant-infected hearts and reovirus-infected ileum were pooled in three separate reactions for xGen hybridization capture. Two rounds of hybridization capture using the xGen enrichment protocol were performed for every reaction to enrich viral transcripts. Amplification was performed for a total of 18 PCR cycles after the first round of capture. Fifty percent of the amplified product was used for the second round of hybridization capture, and amplification was performed for a total of five PCR cycles after the second round of enrichment. Post-enrichment products were pooled and sequenced on Illumina Mini-seq for ileum libraries and NextSeq 500 for heart libraries.

Sample preparation for Visium spatial transcriptomics

Whole hearts and intestinal ileum were isolated using aseptic techniques and placed in ice-cold sterile HBSS (without calcium and magnesium chloride; Gibco, 14175-095). Blood and other contamination were carefully removed by perfusing the tissues with fresh HBSS. Fresh tissues were immediately embedded in OCT media (SAKURA, 25608-930) and frozen in a liquid-nitrogen-cooled isopentane (EMD Millipore, MX0760) bath for spatial transcriptomics experiments. The tissue blocks were cut into 10- μm sections using Thermo Fisher Scientific CryoStar NX50 cryostat and mounted on Visium Gene Expression slides (10x Genomics), which were pre-cooled to -20°C and used for the Visium Spatial Gene Expression experiment.

Visium spatial transcriptomics library preparation

We used the Visium Spatial Gene Expression (10x Genomics) platform for the spatial transcriptomics experiments. Tissue sections from fresh-frozen hearts (mock-infected and reovirus-infected at 4 dpi and 7 dpi) and ileum (mock-infected and reovirus-infected at 1 dpi and 4 dpi) were mounted with one section per capture area on individual Visium Gene Expression slides. These sections are then fixed in pre-chilled methanol for 30 minutes and then H&E stained and imaged, which is later used by the 10x Genomics Space Ranger (version 1.0.0) software to detect the spots that are covered by the tissue. The optimal permeabilization

time for 10- μm -thick sections was found to be 18 minutes for the heart and 12 minutes for the ileum using the 10x Genomics Visium Tissue Optimization kit. Spatially tagged cDNA libraries were built using the 10x Genomics Visium Spatial Gene Expression 3' Library Construction V1 Kit. H&E-stained heart tissue sections were imaged using Zeiss PALM MicroBeam laser capture microdissection system at $\times 20$ objective, and the images were stitched and processed using Fiji ImageJ (version 1.52p) software. cDNA libraries were sequenced on an Illumina NextSeq 500/550 using 150-cycle high-output kits (Read 1 = 28, Read 2 = 120, Index 1 = 10 and Index 2 = 10) for ileum and on an Illumina NextSeq 2K (P2 flow cell) using the 100-cycle kit (Read 1 = 28, Read 2 = 96, Index 1 = 10 and Index 2 = 10) for the heart samples. Fiducial frames around the capture area on the Visium slide were aligned manually, and spots covering the tissue were selected using Loupe Browser 4.0.0 software (10x Genomics). Sequencing data were then aligned to a combined mouse and reovirus reference genome (described below) using the Space Ranger 1.0.0 (10x Genomics) pipeline to derive a feature spot-barcode expression matrix. Visium slide number V19B23-046 was used for spatial transcriptomics experiment on mice hearts (mock-infected 4 dpi: capture area D1, reovirus-infected 4 dpi: capture area B1, mock-infected 7 dpi: capture area C1 and reovirus-infected 7 dpi: capture area A1). Visium slide number V19B23-045 was used for spatial transcriptomics experiment on mice ileum tissue (mock-infected 1 dpi: capture area D1, reovirus-infected 1 dpi: capture area B1, mock-infected 4 dpi: capture area C1 and reovirus-infected 4 dpi: capture area A1).

Sample preparation for Slide-seq spatial transcriptomics

Whole hearts were isolated using aseptic technique and placed in ice-cold sterile HBSS (without calcium and magnesium chloride; Gibco, 14175-095). Blood and other contamination were carefully removed by perfusing the tissues with fresh HBSS. Fresh tissues were immediately embedded in OCT media (SAKURA, 25608-930) and frozen in a liquid-nitrogen-cooled isopentane (EMD Millipore, MX0760) bath for spatial transcriptomics experiments. The tissue blocks were cut into 10- μm sections using Thermo Fisher Scientific CryoStar NX50 cryostat and mounted on a Curio Seeker Tile (A0004_043, Curio Bioscience). A barcode whitelist and a barcode position file for the corresponding tile were provided by Curio Bioscience.

Slide-seq spatial transcriptomics library preparation

Slide-seq spatial transcriptomics experiment was performed using the Curio Seeker Kit (Curio Bioscience) according to manufacturer instructions. In brief, a tissue section from a fresh-frozen reovirus-infected heart at 7 dpi was mounted on a 3-mm \times 3-mm spatially indexed bead surface (Curio Seeker Kit, A0004_043, Curio Bioscience). After RNA hybridization and reverse transcription, the tissue section was digested, and the beads were removed from the glass tile and resuspended. Second strand synthesis was then performed by semi-random priming followed by cDNA amplification. A sequencing library was then prepared using the Nextera XTDNA sample preparation kit. The library was sequenced on an Illumina NextSeq 2K (P3 flow cell) using the 100-cycle kit (Read 1 = 50 bp, Read 2 = 80 and Index 1 = 10). The data were aligned to a combined mouse and reovirus reference genome (described below) using the STAR Solo (version 2.7.9a) pipeline to derive a feature \times bead barcode expression matrix.

Slide-seq data pre-processing and analysis

Slide-seq count matrix and the position information for every bead barcode were loaded into an AnnData object using Scanpy (version 1.9.1). After filtering the beads with fewer than 50 transcripts detected and after removing genes detected in fewer than ten beads, we log-normalized the Slide-seq expression data and computed principal components (PCs) using highly variable genes (minimum dispersion = 0.2, minimum mean expression = 1.0). The transcriptomes were then clustered, and differential gene expression analysis (two-sided Wilcoxon test) was performed to label bead clusters. Neighborhood

enrichment permutation test was performed using Squidpy⁴⁸ (version 1.2.2). Cell2location⁴⁹ (version 0.1) was used for deconvolution of the Slide-seq transcriptomes using the scRNAseq as a reference. Genes in the reference were filtered with cell_count_cutoff = 5, cell_percent_cutoff = 0.03 and nonz_mean_cutoff = 1.12 to select for highly expressed markers of rare cell types while removing most uninformative genes. Cell type signatures were determined using NB regression and used for spatial mapping of scRNAseq cell types on Slide-seq data with hyperparameters N_cells_per_location = 1 and detection_alpha = 20.

Reference genome and annotation

Mus musculus genome and gene annotations (assembly GRCm38) were downloaded from the Ensembl genome browser, and reovirus strain T1L genome and gene annotations were downloaded and compiled from the National Center of Biotechnology Information (NCBI) browser. We have shared reovirus genome sequence and annotation files on figshare with the identifier <https://doi.org/10.6084/m9.figshare.c.5726372>. Genomes were processed using the Cell Ranger version 3.0.0 (10x Genomics) pipeline's mkref command.

scRNA-seq data processing and visualization

Cells with fewer than 200 unique genes or more than 25% of transcripts aligning to mitochondrial genes were removed. After quality control, we captured 6,596, 7,096 and 3,483 single-cell transcriptomes from mock-infected hearts; 5,970, 5,086 and 3,453 single-cell transcriptomes from reovirus WT-infected hearts; and 5,354, 7,462 and 3,955 cells from reovirus mutant K287T-infected hearts at 4 dpi, 7 dpi and 10 dpi, respectively. The single-cell transcriptomes were log-transformed and normalized using the Scanpy package verison 1.8.1 (ref. ⁵⁰). We used Scanpy to choose the highly variable genes with min_disp = 0.5 and max_mean = 3 thresholds. We then performed mean centering and scaling while regressing out total unique molecular identifier (UMI) counts, percent mitochondrial transcripts, S score and G2M score, followed by principal component analysis (PCA) to reduce the dimensions of the data to the top 20 PCs. Uniform manifold approximation and projection (UMAP) and the nearest neighbor (NN) graph were initialized in this PCA space using the first 20 PCs. The cells were then clustered using the Leiden method with multiple values of clustering resolution to get fine (resolution = 0.5) and broad (resolution = 0.3) cell type clusters. Cell-type-specific canonical gene markers along with differentially expressed genes (Wilcoxon method) for each cluster were used to assign cell type labels. Normalized gene expression was visualized on DotPlots, UMAP plots and Violin plots across cell type groups. All visualization was performed using Scanpy (version 1.8.1), seaborn (version 0.11.1) and matplotlib (version 3.3.4) packages. A few cell type clusters representing cell states of the same cell type were grouped into broad cell type groups using cell type marker genes and then used for downstream analysis. Differential gene expression analysis (DGEA) was performed using the rank_gene_groups function in Scanpy with the Wilcoxon statistical method. All gene module scores were calculated using the score_genes function in Scanpy.

Reclustering and analysis of endothelial cells, T cells, fibroblasts, and cardiomyocytes

Normalized gene expression for a specific cell type group was extracted from the combined scRNA-seq dataset. We used Scanpy to reselect the highly variable genes within that cell type group with min_disp=0.5 and max_mean=3 thresholds. We then performed mean centering and scaling while regressing out total UMI counts, percent mitochondrial transcripts, Sscore, and G2M score, followed by principal component analysis (PCA) to reduce the dimensions of the data to the top 20 principal components (PCs). Uniform Manifold Approximation and Projection (UMAP) and the Nearest Neighbor (NN) graph were initialized in this PCA space using the first 20 PCs. The cells were then reclustered using the Leiden method (resolution=0.5 for endothelial cells, Resolution=0.3 for T cells, Resolution=0.2 for fibroblasts, and Resolution=0.3 for cardiomyocytes) to get

cell type subclusters. Differentially expressed genes (wilcoxon method) for each subcluster were then used to assign cell subtype labels. Subclusters representing doublets and expressing markers of multiple cell types were then removed from the analysis. Normalized gene expression for differentially expressed genes and genes of interest was visualized on DotPlots and UMAP plots across celltype subgroups. All visualization was performed using scanpy (v1.8.1), seaborn (v0.11.1), and matplotlib (v3.3.4) packages. DGEA was performed using the rank_gene_groups function in Scanpy with the Wilcoxon statistical method. All gene module scores were calculated using the score_genes function in Scanpy.

Spatial transcriptomics data processing, integration, analysis and visualization

Spatial transcriptomics data from barcoded spatial spots from four heart sections were log-normalized using the Scanpy package (version 1.8.1). The Scanpy package was then used to select highly variable genes for spatial transcriptomics data with min_disp = 0.5 and max_mean = 3 thresholds. We then performed mean centering and scaling while regressing out total UMI counts, percent mitochondrial UMIs, S score and G2M score, followed by PCA on the spot gene expression matrix, and reduced the dimensions of the data to the top 20 PCs. UMAP and the NN graph were initialized in this PCA space. The spots were then clustered using the Leiden method with multiple values of clustering resolution. The method returned spot clusters representing different tissue regions, which were then visualized on H&E images as spatial transcriptomics maps for individual samples to assign anatomical regions. Normalized gene expression was visualized on spatial transcriptomics maps for all tissue sections. Spot clusters representing the same tissue regions were grouped into broad anatomical region groups using marker genes and then used for downstream analysis. The cell2location (version 0.1) deconvolution method compactible with Scanpy and scvi-tools⁵¹ (version 0.16.4) package was used for integration of spatial transcriptomics data with time-matched scRNA-seq data, and cell type prediction values for spatial transcriptomics spots were estimated for the infected heart at 7 dpi. DGEA for anatomical regions was performed using the rank_gene_groups function in Scanpy with the Wilcoxon statistical method.

Viral transcript sequencing data processing, filtering and visualization

Enriched viral transcript data were aligned to a combined mouse and reovirus T1L genome for all infected samples. Viral UMI counts were taken from the combined expression matrices and added as metadata in the host gene expression data. Viral UMI counts in empty droplets, droplets with low-quality cells (<200 host UMI counts) and droplets with viable cells (\geq 200 host UMI counts) were sorted by viral UMI and visualized on a histogram to filter out the cell-free ambient viral RNA enriched in the hybridization protocol. Using the distribution of viral UMI counts in empty droplets, thresholds of two viral UMIs and five viral UMIs were used to identify infected cells in the heart and ileum, respectively. Viral transcripts in the infected cells were then visualized on a DotPlot to determine viral tropism in tissues.

GO term enrichment analysis for scRNA-seq and spatial transcriptomics

GO term enrichment analysis was performed on differentially expressed genes using gseapy (version 0.10.4) wrapper package⁵². Differentially expressed genes (two-sided Wilcoxon test, log fold change threshold = 2.0, $P < 10^{-4}$ for scRNA-seq cells and log fold change threshold = 0.5, $P < 10^{-2}$ for spatial transcriptomics spots) were selected and used for GO term enrichment analysis using GO_Biological_Processes_2021 gene sets in enrichr command⁵³. The enriched GO terms of interest were selected and visualized on a bar plot. The genes associated with GO terms of interested were used to calculate module scores using the score_genes command in Scanpy.

Sample preparation for RNA FISH, immunofluorescence and histology

Whole hearts were isolated using aseptic technique and placed in ice-cold sterile HBSS, and then blood was carefully removed by perfusing the hearts with fresh HBSS through the apex. Fresh tissues were immediately embedded in OCT media and frozen in liquid-nitrogen-cooled isopentane, cut into 10- μ m sections using a Thermo Fisher Scientific Microm 550 cryostat and mounted on -20 °C cooled histological glass slides, which were then stored at -80 °C until used.

RNA FISH split probe design and signal amplification using hybridization chain reaction V3

Two-step hybridization strategy with split probe design and hybridization chain reaction (HCR) V3 (ref. ⁵⁴) was used to label up to three transcripts in a single tissue section. Probes were designed using NCBI primer-blast, which uses primer3 for designing internal hybridization oligo and BLASTn to check for binding specificity. We designed 20–21-bp primer pairs for an amplicon length of 40–42 bp (2 \times primer length), primer melting temperature between 57 °C and 63 °C and primer GC content between 35% and 65%. Then, 7–10 sets of reverse complemented forward primers and reverse primers were concatenated to flanking initiator sequence for HCR, ordered from Integrated DNA Technologies with standard desalting purification (Supplementary Table 4). Split probes for each gene target were mixed and diluted in nuclease-free water to create a split probe pool stock solution at 10 μ M total probe concentration for every target. Hairpin pairs labeled with three different fluorophores, namely Alexa Fluor 488, Alexa Fluor 546 and Alexa Fluor 647 (Molecular Instruments; Supplementary Table 5), were used for HCR V3.

RNA FISH experiments

Slides with tissue sections were then brought to room temperature until the OCT melted and were then immediately fixed in 4% paraformaldehyde for 12 minutes at room temperature. After fixation, the sections were washed for 5 minutes in 1 \times PBS twice, incubated for 1 hour in 70% ethanol for tissue permeabilization, washed again for 5 minutes in 1 \times PBS and then used for primary hybridization. Hybridization Buffer (HB) mix was prepared with 2 \times SSC, 5 \times of Denhart solution, 10% ethylene carbonate, 10% dextran sulfate, 0.01% SDS and 1 μ M of probe pool mix per target for the hybridization reaction. Then, 20 μ l of HB mix (with probes) per section was put on each slide to cover the tissue section, covered with parafilm and incubated overnight at 37 °C inside a humidifying chamber for primary hybridization. After primary hybridization, parafilm was removed, and slides were washed in Hybridization Wash Buffer-1 (0.215 M NaCl, 0.02 M Tris HCl pH 7.5 and 0.005 M EDTA) for 20–30 minutes at 48 °C. Amplification Buffer (AB) mix was prepared with 2 \times SSC, 5 \times of Denhart solution, 10% dextran sulfate, 0.01% SDS and 0.06 μ M of HCR hairpins for the amplification reaction. Next, 2 μ l of each fluorophore-labeled hairpins at 3 μ M corresponding to the target genes were mixed, incubated at 95 °C for 1.5 minutes, covered in aluminum foil and left to cool down at room temperature for 30 minutes to form hairpins before adding it to AB mix. Then, 20 μ l of AB mix per section was put on each slide to cover the tissue section, covered with parafilm and incubated overnight at room temperature in the dark for signal amplification. After signal amplification, parafilm was removed, and slides were washed in 5 \times SSCT buffer twice for 30–40 minutes and then twice for 10 minutes. The slides were then carefully cleaned with Kimwipe and treated with Ready Probes Auto-fluorescence Quenching Reagent Mix (Thermo Fisher Scientific, R37630) for 5 minutes and washed three times in 1 \times PBS. Finally, tissue sections were then counterstained with DAPI for 10 minutes at room temperature and washed for 5 minutes in 1 \times PBS twice, excess PBS was cleaned using Kimwipe, and sections were immediately mounted on coverslips using Slowfade antifade media, left overnight for treatment and imaged the next day on a Zeiss Axio Observer Z1 Microscope using a Hamamatsu ORCA Fusion Gen III Scientific CMOS camera. smFISH images were shading-corrected, stitched, rotated, thresholded and exported as TIFF files using ZEN 3.1 software (blue edition).

Immunofluorescence assays

Slides with tissue sections were brought from -80 °C freezer and heated for 1 minute at 37 °C until the OCT melted and were then immediately dipped in pre-chilled methanol at -20 °C for 30 minutes. After fixation, the slides were then rehydrated to Milli-Q water for 2 minutes and then washed twice in 1 \times PBS. Samples then underwent an antigen retrieval step via incubation in 1 \times citrate buffer for 10–15 minutes at 95 °C. Samples were then permeabilized in 0.1% Triton X-100 in 1 \times PBS for 15 minutes, washed three times in 0.05% Tween 20 in PBS (TBST), blocked for 1 hour at room temperature in blocking buffer (1% BSA and 10% normal donkey serum in PBS). Then, 20 μ l of primary antibodies diluted in antibody solution (1% BSA in PBS) was added onto the slides, which were covered with parafilm and incubated in a humidifying chamber overnight at 4 °C. Primary antibodies used were rabbit anti-reovirus VM1:VM6 polyclonal sera (1:30,000), rat anti-caspase-1 monoclonal antibody (1:200, clone: 5B10, 14-9832-82, Invitrogen), rabbit anti-cleaved caspase-1 (Asp297) (1:200, 4199T, Cell Signaling Technology) and rabbit anti-cleaved gasdermin D (Asp275) (1:200, 36425S, Cell Signaling Technology). Cleaved caspase-1 and cleaved gasdermin D antibodies were purchased as a part of Pyroptosis Antibody Sampler Kit (43811T, Cell Signaling Technology). After overnight primary incubation, samples were washed three times in PBS and then incubated in secondary antibodies diluted in blocking solution for 2 hours at room temperature. The secondary antibodies were donkey anti-rabbit Alexa Fluor 488 (1:500, 711-545-152, Jackson ImmunoResearch); donkey anti-rabbit Alexa Fluor 647 (1:500, 711-605-152, Jackson ImmunoResearch); and donkey anti-rat Alexa Fluor 647 (1:500, ab150155, Abcam). Lastly, samples were washed thrice in PBS for 10 minutes with shaking, counterstained with DAPI and mounted in Prolong antifade mounting media. Images were acquired on a Zeiss Axio Observer Z1 Microscope using a Hamamatsu ORCA Fusion Gen III Scientific CMOS camera. Immunostaining images were shading corrected, stitched, rotated, thresholded and exported as TIFF files using ZEN 3.1 software (blue edition).

Processing and quantification of histology, RNA FISH and immunofluorescence images

Image analysis and processing for histology, immunofluorescence and RNA FISH images was done manually in ZEN 3.1 software (blue edition) and Fiji ImageJ. Whole heart H&E images were thresholded using non-linear adjustments ($\gamma = 0.45$) applied across entire images using ZEN 3.1 blue software. For area quantifications from H&E-stained histology images, three-color RGB images were opened in ImageJ. The images were converted to greyscale 8-bit images and thresholded to detect the entire tissue section area. Sites of inflammation were manually selected for calculating the inflammation percentage in the tissue. For RNA FISH images, the images with DAPI counterstain channel were manually thresholded to segment nuclei. Holes in nuclei segmentation mask were filled, and morphological opening was performed to remove noise. The segmentation was enhanced using watershed algorithm followed by a morphological opening operation. For RNA FISH images, individual channels TIFF files exported from ZEN 3.1 software were opened in ImageJ and converted to 8-bit images. Images were manually thresholded using linear adjustments ($\gamma = 1.0$) applied across entire images to detect RNA-labeled cells, and morphological opening was performed to remove noise. The nuclei and cells were counted in all images using the Analyze Particle function in ImageJ. For immunofluorescence images, individual channels were thresholded using linear adjustments ($\gamma = 1.0$) applied across entire images. Thresholded images were loaded in Fiji ImageJ and converted to 8-bit images. The grayscale images for individual channels were then used to segment signal using same thresholds across all tissue sections to get selections for area quantifications. The tissue border was manually removed from the fluorescence channels when calculating the area of interest. Entire hearts were manually selected using DAPI

channel to calculate total area of the tissue. Any changes to brightness and contrast were applied equally across the entire image for visibility of fluorescence signal.

Reporting summary

Further information on research design is available in the Nature Research Reporting Summary linked to this article.

Data availability

The authors declare that all sequencing data supporting the findings of this study have been deposited in the NCBI Gene Expression Omnibus (GEO)⁵⁵ with series accession number [GSE189636](#). Sequencing data for high-resolution Slide-seq spatial transcriptomics have been deposited in the GEO with series accession number [GSE211096](#). Raw and processed H&E-stained tissue images and tissue spot alignment files matched to spatial transcriptomics datasets have been made publicly available on figshare: <https://doi.org/10.6084/m9.figshare.c.5726372> (ref. ⁵⁶). *Mus musculus* genome and gene annotations (assembly [GRCh38](#)) were downloaded from the Ensembl genome browser, and reovirus strain T1L genome and gene annotations were downloaded and compiled from the NCBI browser. We have shared reovirus genome sequence and annotation files on figshare: <https://doi.org/10.6084/m9.figshare.c.5726372> (ref. ⁵⁶). All other data supporting the findings in this study are included in the main article and associated files. Source data are provided with this paper.

Code availability

Scripts to reproduce the analysis presented in this study have been deposited on GitHub (https://github.com/madhavmantri/reovirus_induced_myocarditis).

References

- Pollack, A., Kontorovich, A. R., Fuster, V. & Dec, G. W. Viral myocarditis—diagnosis, treatment options, and current controversies. *Nat. Rev. Cardiol.* **12**, 670–680 (2015).
- Rose, N. R. Viral myocarditis. *Curr. Opin. Rheumatol.* **28**, 383–389 (2016).
- Yajima, T. & Knowlton, K. U. Viral myocarditis from the perspective of the virus. *Circulation* **119**, 2615–2624 (2009).
- Tschöpe, C. et al. Myocarditis and inflammatory cardiomyopathy: current evidence and future directions. *Nat. Rev. Cardiol.* **18**, 169–193 (2021).
- Woodruff, J. F. Viral myocarditis. A review. *Am. J. Pathol.* **101**, 425–484 (1980).
- Lasrado, N. & Reddy, J. An overview of the immune mechanisms of viral myocarditis. *Rev. Med. Virol.* **30**, 1–14 (2020).
- Sherry, B., Schoen, F. J., Wenske, E. & Fields, B. N. Derivation and characterization of an efficiently myocarditic reovirus variant. *J. Virol.* **63**, 4840–4849 (1989).
- Boehme, K. W., Lai, C. M. & Dermody, T. S. Mechanisms of reovirus bloodstream dissemination. *Adv. Virus Res.* **87**, 1–35 (2013).
- Guo, Y. et al. The multi-functional reovirus σ3 protein is a virulence factor that suppresses stress granule formation and is associated with myocardial injury. *PLoS Pathog.* **17**, e1009494 (2021).
- Swirski, F. K. & Nahrendorf, M. Cardioimmunology: the immune system in cardiac homeostasis and disease. *Nat. Rev. Immunol.* **18**, 733–744 (2018).
- Sherry, B., Li, X. Y., Tyler, K. L., Cullen, J. M. & Virgin, H. W. Lymphocytes protect against and are not required for reovirus-induced myocarditis. *J. Virol.* **67**, 6119–6124 (1993).
- Phillips, M. B., Dina Zita, M., Howells, M. A., Weinkopff, T. & Boehme, K. W. Lymphatic type 1 interferon responses are critical for control of systemic reovirus dissemination. *J. Virol.* **95**, e02167-20 (2021).
- Holm, G. H. et al. Interferon regulatory factor 3 attenuates reovirus myocarditis and contributes to viral clearance. *J. Virol.* **84**, 6900–8 (2010).
- Schaum, N. et al. Single-cell transcriptomics of 20 mouse organs creates a Tabula Muris. *Nature* **562**, 367–372 (2018).
- Kalucka, J. et al. Single-cell transcriptome atlas of murine endothelial cells. *Cell* **180**, 764–779 (2020).
- Tokunaga, R. et al. CXCL9, CXCL10, CXCL11/CXCR3 axis for immune activation—a target for novel cancer therapy. *Cancer Treat. Rev.* **63**, 40–47 (2018).
- Woudstra, L., Juffermans, L. J. M., van Rossum, A. C., Niessen, H. W. M. & Krijnen, P. A. J. Infectious myocarditis: the role of the cardiac vasculature. *Heart Fail. Rev.* **23**, 583–595 (2018).
- Mai, J., Virtue, A., Shen, J., Wang, H. & Yang, X. F. An evolving new paradigm: endothelial cells—conditional innate immune cells. *J. Hematol. Oncol.* **6**, 61 (2013).
- Chávez-Galán, L., Arenas-Del Angel, M. C., Zenteno, E., Chávez, R. & Lascurain, R. Cell death mechanisms induced by cytotoxic lymphocytes. *Cell. Mol. Immunol.* **6**, 15–25 (2009).
- Leuschner, F. et al. Silencing of CCR2 in myocarditis. *Eur. Heart J.* **36**, 1478–1488 (2015).
- Miteva, K. et al. Mesenchymal stromal cells modulate monocytes trafficking in coxsackievirus B3-induced myocarditis. *Stem Cells Transl. Med.* **6**, 1249–1261 (2017).
- Barton, P. J. R. et al. Increased expression of extracellular matrix regulators TIMP1 and MMP1 in deteriorating heart failure. *J. Heart Lung Transplant.* **22**, 738–744 (2003).
- Yang, X., Bam, M., Becker, W., Nagarkatti, P. S. & Nagarkatti, M. Long noncoding RNA AW112010 promotes the differentiation of inflammatory T cells by suppressing IL-10 expression through histone demethylation. *J. Immunol.* **205**, 987–993 (2020).
- Swertfeger, D. K., Witte, D. P., Stuart, W. D., Rockman, H. A. & Harmony, J. A. K. Apolipoprotein J/clusterin induction in myocarditis: a localized response gene to myocardial injury. *Am. J. Pathol.* **148**, 1971–1983 (1996).
- Szalay, G. et al. Ongoing coxsackievirus myocarditis is associated with increased formation and activity of myocardial immunoproteasomes. *Am. J. Pathol.* **168**, 1542–1552 (2006).
- Van Der Borght, K. et al. Myocarditis elicits dendritic cell and monocyte infiltration in the heart and self-antigen presentation by conventional type 2 dendritic cells. *Front. Immunol.* **9**, 2714 (2018).
- Stewart, M. J., Smoak, K., Blum, M. A. & Sherry, B. Basal and reovirus-induced beta interferon (IFN-β) and IFN-β-stimulated gene expression are cell type specific in the cardiac protective response. *J. Virol.* **79**, 2979–2987 (2005).
- Duer, G. D. et al. Metallothioneins 1 and 2 modulate inflammation and support remodeling in ischemic cardiomyopathy in mice. *Mediators Inflamm.* **2016**, 7174127 (2016).
- Bogomolovas, J. et al. Induction of Ankrd1 in dilated cardiomyopathy correlates with the heart failure progression. *Biomed. Res. Int.* **2015**, 273936 (2015).
- Yamada, S. et al. Spatiotemporal single-cell analysis reveals critical roles of mechano-sensing genes at the border zone in remodeling after myocardial infarction. Preprint at <https://www.researchsquare.com/article/rs-620498/v1> (2021).
- Rodrigues, S. G. et al. Slide-seq: a scalable technology for measuring genome-wide expression at high spatial resolution. *Science* **363**, 1463–1467 (2019).
- Stickels, R. R. et al. Highly sensitive spatial transcriptomics at near-cellular resolution with Slide-seqV2. *Nat. Biotechnol.* **39**, 313–319 (2020).
- Jun, H. O. et al. Clusterin protects H9c2 cardiomyocytes from oxidative stress-induced apoptosis via Akt/GSK-3β signaling pathway. *Exp. Mol. Med.* **43**, 53–61 (2010).

34. Witt, E. et al. Correlation of gene expression and clinical parameters identifies a set of genes reflecting LV systolic dysfunction and morphological alterations. *Physiol. Genomics* **51**, 356–367 (2019).
35. Houweling, A. C., Van Borren, M. M., Moorman, A. F. M. & Christoffels, V. M. Expression and regulation of the atrial natriuretic factor encoding gene *Nppa* during development and disease. *Cardiovasc. Res.* **67**, 583–593 (2005).
36. Gupta, S., Markham, D. W., Drazner, M. H. & Mammen, P. P. A. Fulminant myocarditis. *Nat. Clin. Pract. Cardiovasc. Med.* **5**, 693–706 (2008).
37. Mantri, M. et al. Spatiotemporal single-cell RNA sequencing of developing chicken hearts identifies interplay between cellular differentiation and morphogenesis. *Nat. Commun.* **12**, 1771 (2021).
38. Asp, M. et al. A spatiotemporal organ-wide gene expression and cell atlas of the developing human heart. *Cell* **179**, 1647–1660 (2019).
39. Kuppe, C. et al. Spatial multi-omic map of human myocardial infarction. *Nature* **608**, 766–777 (2022).
40. Lindner, D. et al. Association of cardiac infection with SARS-CoV-2 in confirmed COVID-19 autopsy cases. *JAMA Cardiol.* **5**, 1281–1285 (2020).
41. Bräuninger, H. et al. Cardiac SARS-CoV-2 infection is associated with pro-inflammatory transcriptomic alterations within the heart. *Cardiovasc. Res.* **118**, 542–555 (2021).
42. Onyimba, J. A. et al. The innate immune response to coxsackievirus B3 predicts progression to cardiovascular disease and heart failure in male mice. *Biol. Sex Differ.* **2**, 2 (2011).
43. Coronado, M. J. et al. Testosterone and interleukin-1 β increase cardiac remodeling during coxsackievirus B3 myocarditis via serpin A 3n. *Am. J. Physiol. Heart Circ. Physiol.* **302**, H1726–H1736 (2012).
44. Lasrado, N., Borcherding, N., Arumugam, R., Starr, T. K. & Reddy, J. Dissecting the cellular landscape and transcriptome network in viral myocarditis by single-cell RNA sequencing. *iScience* **25**, 103865 (2022).
45. Baty, C. J. & Sherry, B. Cytopathogenic effect in cardiac myocytes but not in cardiac fibroblasts is correlated with reovirus-induced acute myocarditis. *J. Virol.* **67**, 6295–6298 (1993).
46. Stewart, M. J., Blum, M. A. & Sherry, B. PKR's protective role in viral myocarditis. *Virology* **314**, 92–100 (2003).
47. Miyamoto, S. D. et al. Cardiac cell-specific apoptotic and cytokine responses to reovirus infection: determinants of myocarditic phenotype. *J. Card. Fail.* **15**, 529–539 (2009).
48. Palla, G. et al. Squidpy: a scalable framework for spatial omics analysis. *Nat. Methods* **19**, 171–178 (2022).
49. Kleshchevnikov, V. et al. Cell2location maps fine-grained cell types in spatial transcriptomics. *Nat. Biotechnol.* **40**, 661–671 (2022).
50. Wolf, F. A., Angerer, P. & Theis, F. J. SCANPY: large-scale single-cell gene expression data analysis. *Genome Biol.* **19**, 15 (2018).
51. Gayoso, A. et al. A Python library for probabilistic analysis of single-cell omics data. *Nat. Biotechnol.* **40**, 163–166 (2022).
52. Subramanian, A. et al. Gene set enrichment analysis: a knowledge-based approach for interpreting genome-wide expression profiles. *Proc. Natl Acad. Sci. USA* **102**, 15545–15550 (2005).
53. Xie, Z. et al. Gene set knowledge discovery with Enrichr. *Curr. Protoc.* **1**, e90 (2021).
54. Choi, H. M. T. et al. Third-generation *in situ* hybridization chain reaction: multiplexed, quantitative, sensitive, versatile, robust. *Development* **145**, dev165753 (2018).
55. Edgar, R. Gene Expression Omnibus: NCBI gene expression and hybridization array data repository. *Nucleic Acids Res.* **30**, 207–210 (2002).

56. Mantri, M. Reovirus-induced-myocarditis. figshare. <https://doi.org/10.6084/m9.figshare.c.5726372> (2021).

Acknowledgements

We would like to thank P. Schweitzer and the Cornell Genomics Center for help with single-cell and spatial sequencing assays; the Cornell Bioinformatics facility for assistance with bioinformatics; and D. M. Sutherland from the laboratory of T. S. Dermody at the University of Pittsburgh for assistance with animal experiments and for providing the anti-reovirus polyclonal sera. We also thank members of the Parker and De Vlaminck laboratories for many valuable discussions. This work was supported by R21AI144557 (to J.S.P. and I.D.V.) and DP2AI138242 (to I.D.V.). M.M. was supported by the CVG Scholar Award from the Center for Vertebrate Genomics at Cornell University. S.T.C. was supported by the National Institutes of Health and National Institute of Allergy and Infectious Diseases Award T32AI145821.

Author contributions

M.M., J.S.P. and I.D.V. designed the study. M.M., M.M.H. and S.T.C. performed the animal experiments. M.M. and M.M.H. performed the scRNA-seq and spatial transcriptomics experiments. M.M., D.W.M. and M.F.Z.W. analyzed the data. M.M. performed histology, RNA FISH and immunostaining experiments and analyzed the images. M.M., J.S.P. and I.D.V. wrote the manuscript. All authors provided feedback and comments.

Competing interests

The authors declare no competing interests.

Additional information

Extended data is available for this paper at <https://doi.org/10.1038/s44161-022-00138-1>.

Supplementary information The online version contains supplementary material available at <https://doi.org/10.1038/s44161-022-00138-1>.

Correspondence and requests for materials should be addressed to John S. L. Parker or Iwijn De Vlaminck.

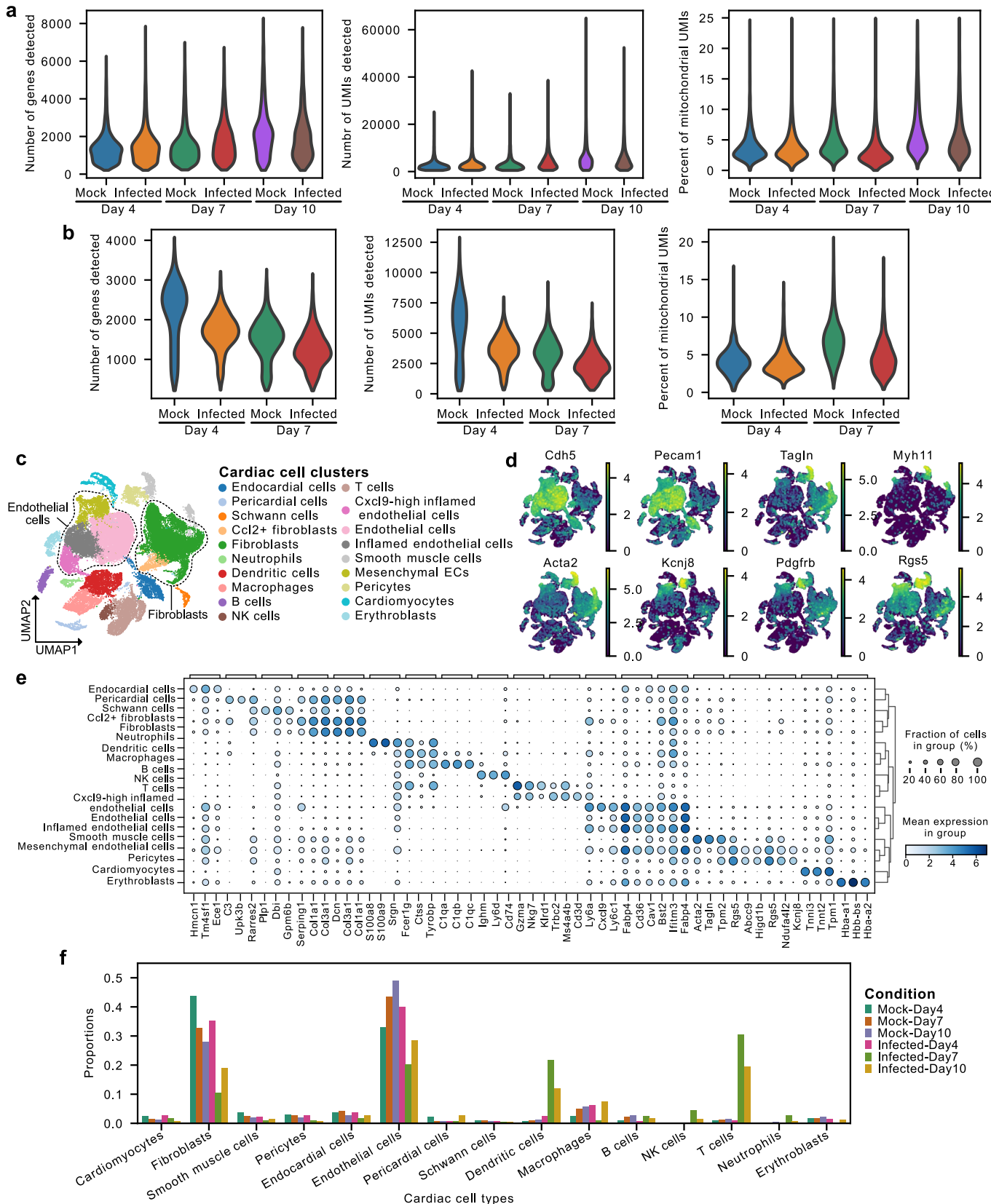
Peer review information *Nature Cardiovascular Research* thanks DeLisa Fairweather, Christer Sylven and the other, anonymous, reviewer(s) for their contribution to the peer review of this work.

Reprints and permissions information is available at www.nature.com/reprints.

Publisher's note Springer Nature remains neutral with regard to jurisdictional claims in published maps and institutional affiliations.

Open Access This article is licensed under a Creative Commons Attribution 4.0 International License, which permits use, sharing, adaptation, distribution and reproduction in any medium or format, as long as you give appropriate credit to the original author(s) and the source, provide a link to the Creative Commons license, and indicate if changes were made. The images or other third party material in this article are included in the article's Creative Commons license, unless indicated otherwise in a credit line to the material. If material is not included in the article's Creative Commons license and your intended use is not permitted by statutory regulation or exceeds the permitted use, you will need to obtain permission directly from the copyright holder. To view a copy of this license, visit <http://creativecommons.org/licenses/by/4.0/>.

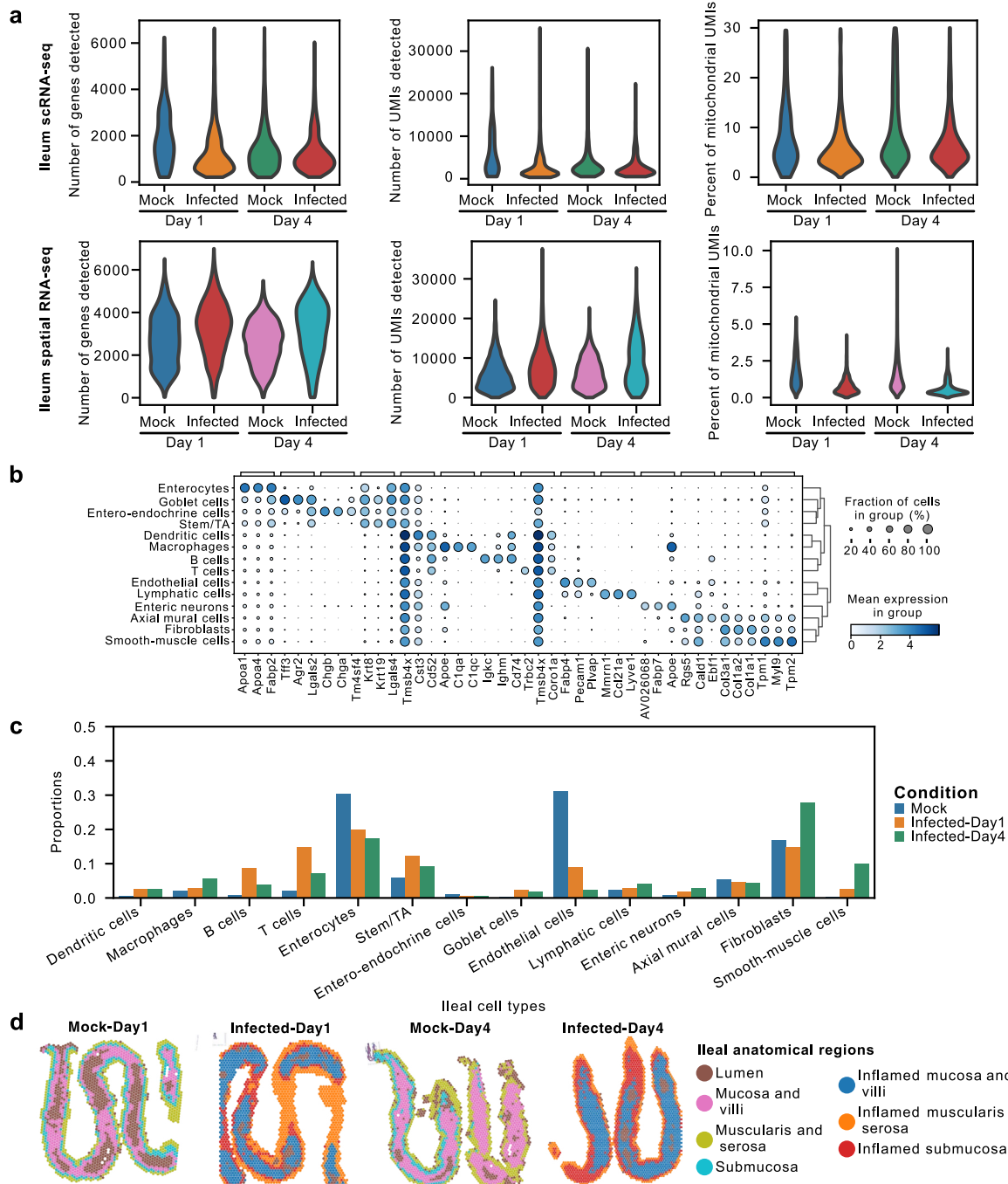
© The Author(s) 2022



Extended Data Fig. 1 | See next page for caption.

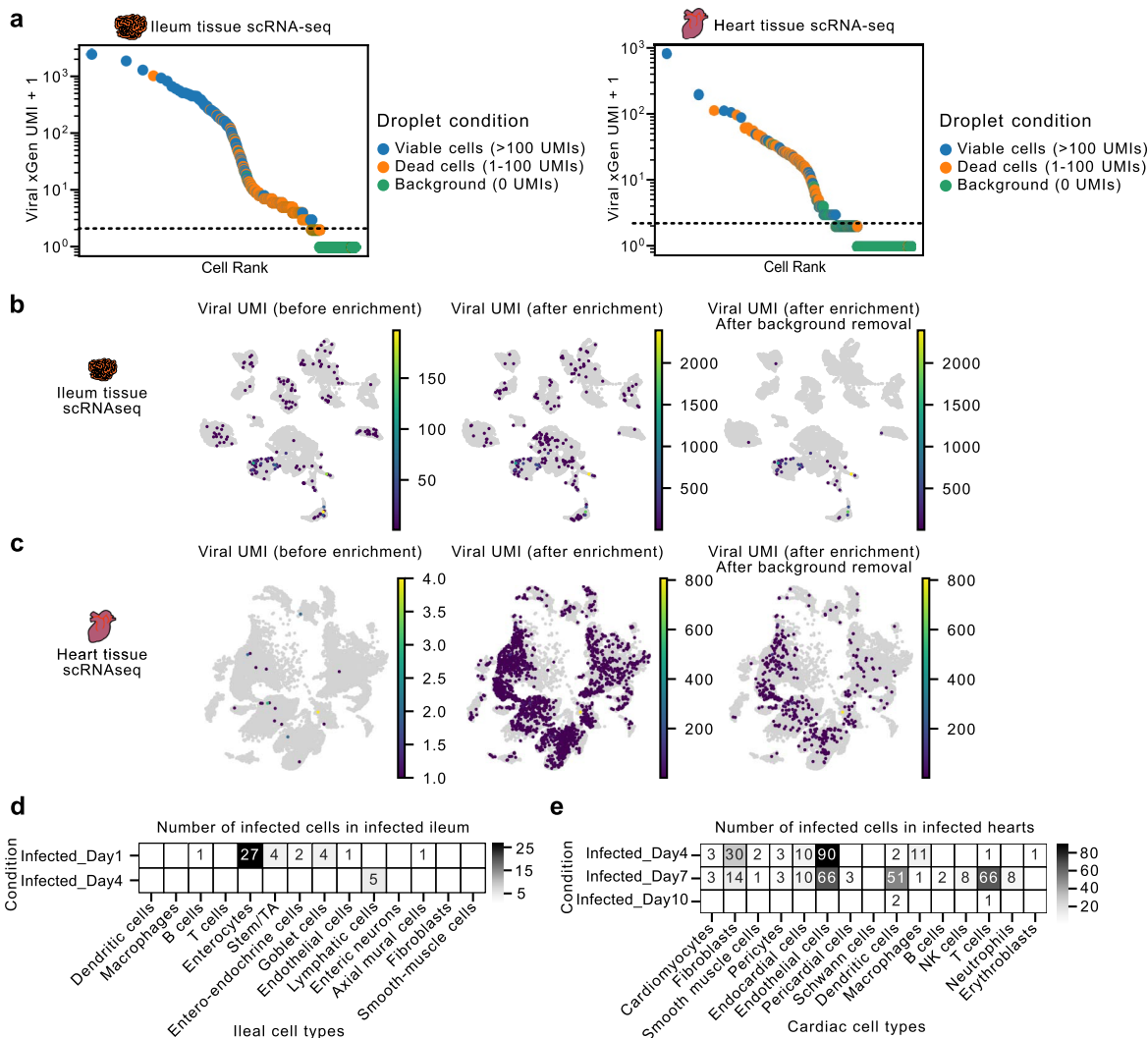
Extended Data Fig. 1 | Single-cell and spatial transcriptomics of cardiac tissue from reovirus-infected neonatal mice. **a)** Number of unique genes detected per cell (left), number of unique transcripts per cell (center), and percentage of mitochondrial transcripts (right) in cardiac scRNA-seq datasets from three stages after infection. **b)** Number of unique genes detected per cell (left), number of unique transcripts per cell (center), and percentage of transcripts from mitochondrial genes (right) in cardiac spatial transcriptomics datasets from two stages after infection. **c)** UMAP plot of 31,684 single-cell transcriptomes from mock-infected and reovirus-infected hearts at 4, 7, and 10 days post-infection (dpi), clustered by gene expression and colored by cardiac cell type. Dotted

lines show the cardiac cell types being grouped as broad endothelial cells and fibroblast cells. **d)** scRNA-seq UMAP plots showing expression of endothelial markers *Cdh5* and *Pecam1*, smooth muscle cell-specific markers *Tagln*, *Myh11*, and *Acta2*, and pericyte markers *Pdgfrb*, *Kcnj8*, and *Rgs5* used to define the *Cdh5* + *Kcnj8* + *Pdgfrb* + mesenchymal endothelial cells (Chen Qi et al. Nature Communications 2016). **e)** Top three differentially expressed genes (two-sided Wilcoxon test, \log_2 fold-change >1.0 and p-value <0.01) for cell types in heart scRNA-seq data. **f)** Bar plot showing the cell type composition changes in scRNA-seq datasets from reovirus-infected and mock-infected mice hearts.



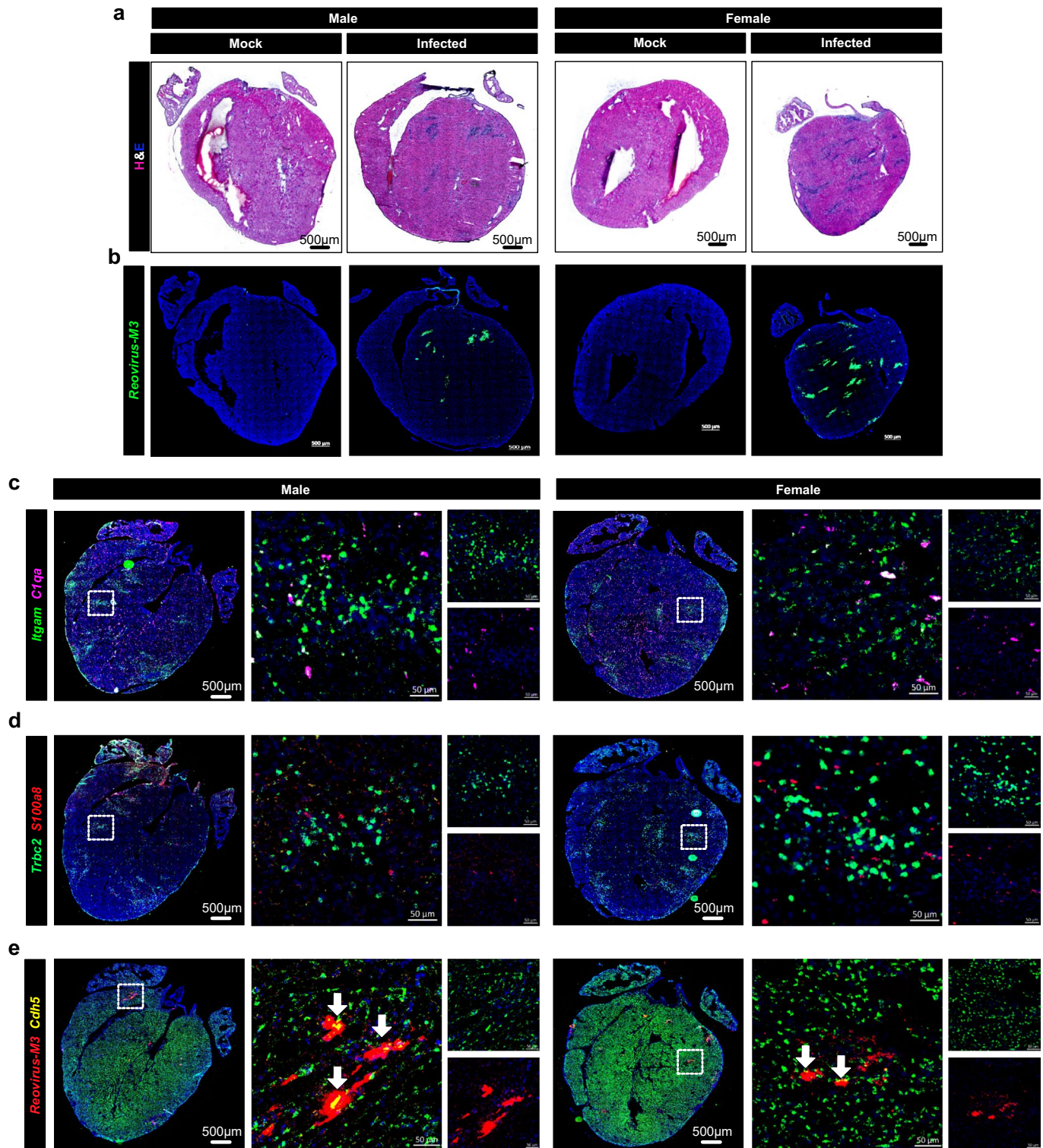
Extended Data Fig. 2 | Single-cell and spatial transcriptomics of ileum tissue from reovirus-infected neonatal mice. **a)** Number of unique genes detected per cell (left), number of unique transcripts per cell (center), and percentage of mitochondrial transcripts (right) in ileum scRNA-seq datasets (top row) and ileum spatial transcriptomics datasets (bottom row) from two stages after infection. **b)** Top-three differentially expressed genes (two-sided Wilcoxon test, \log_2 fold-change >1.0 and p-value <0.01) for cell types in ileum scRNA-seq data.

c) Bar plot showing the cell type composition changes in scRNA-seq datasets from reovirus-infected and mock-infected mice in ileum tissue. Mock sample bar represents the mean cell type proportions for mock ileum samples at 1 and 4 dpi. **d)** Spatial transcriptomics map of ileum tissue sections from mock-infected and reovirus-infected mice at 1 and 4 dpi, colored by clusters representing tissue anatomical regions.



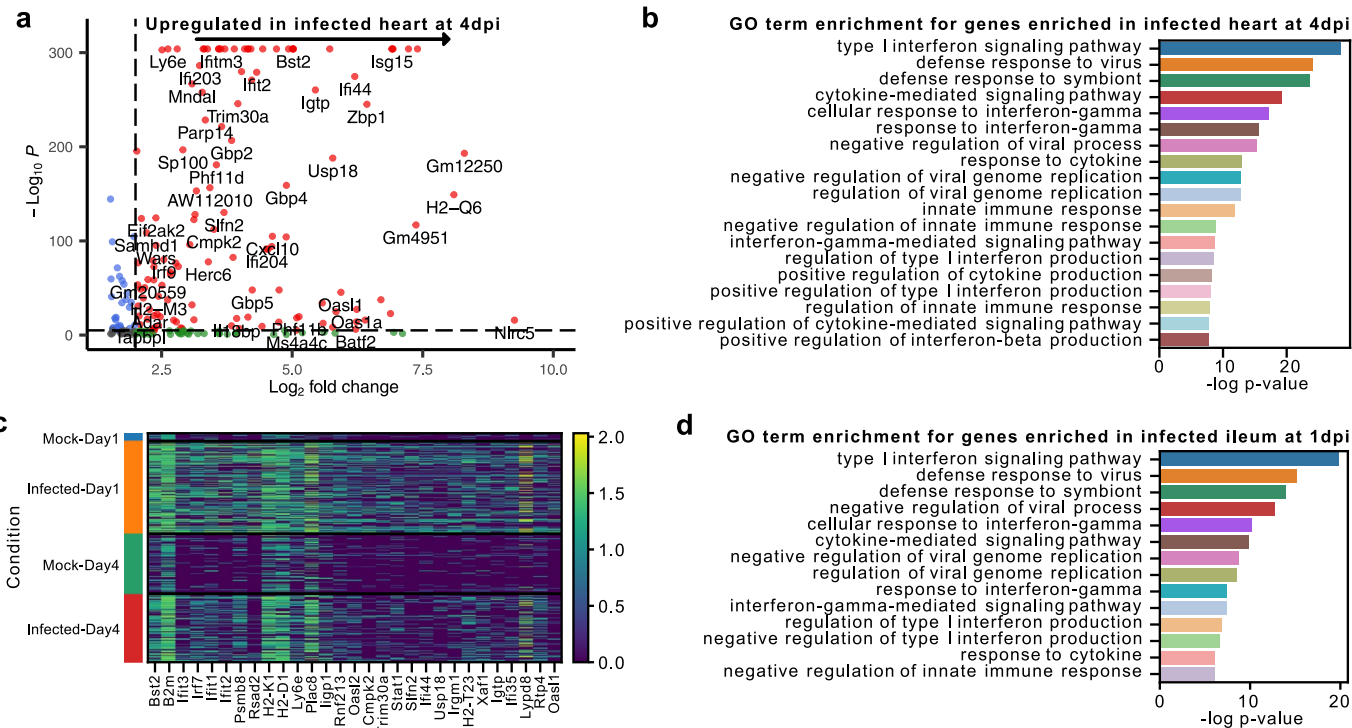
Extended Data Fig. 3 | Enrichment of viral transcripts from single-cell transcriptomics libraries of ileum and heart tissue from reovirus-infected neonatal mice. **a**) Knee plot showing viral UMI counts in the scRNA-seq droplets classified as either empty droplets or with viable/dead cells across ileum (left) and heart (right) scRNA-seq samples. The droplets were labelled using host gene UMI counts detected in scRNA-seq datasets. **b**) scRNA-seq UMAP plots showing total viral UMI counts per cell before xGen enrichment, after xGen viral transcript

enrichment, and after removal of background signal on ileum samples. **c**) scRNA-seq UMAP plots showing total viral UMI counts per cell before xGen enrichment, after xGen viral transcript enrichment, and after removal of background signal on heart samples. **d**) Heatmaps showing counts of infected cells of different ileal cell types across two reovirus-infected ileum samples from 1 and 4 dpi. **e**) Heatmaps showing counts of infected cells of different cardiac cell types across three reovirus-infected heart samples from 4, 7, and 10 dpi.



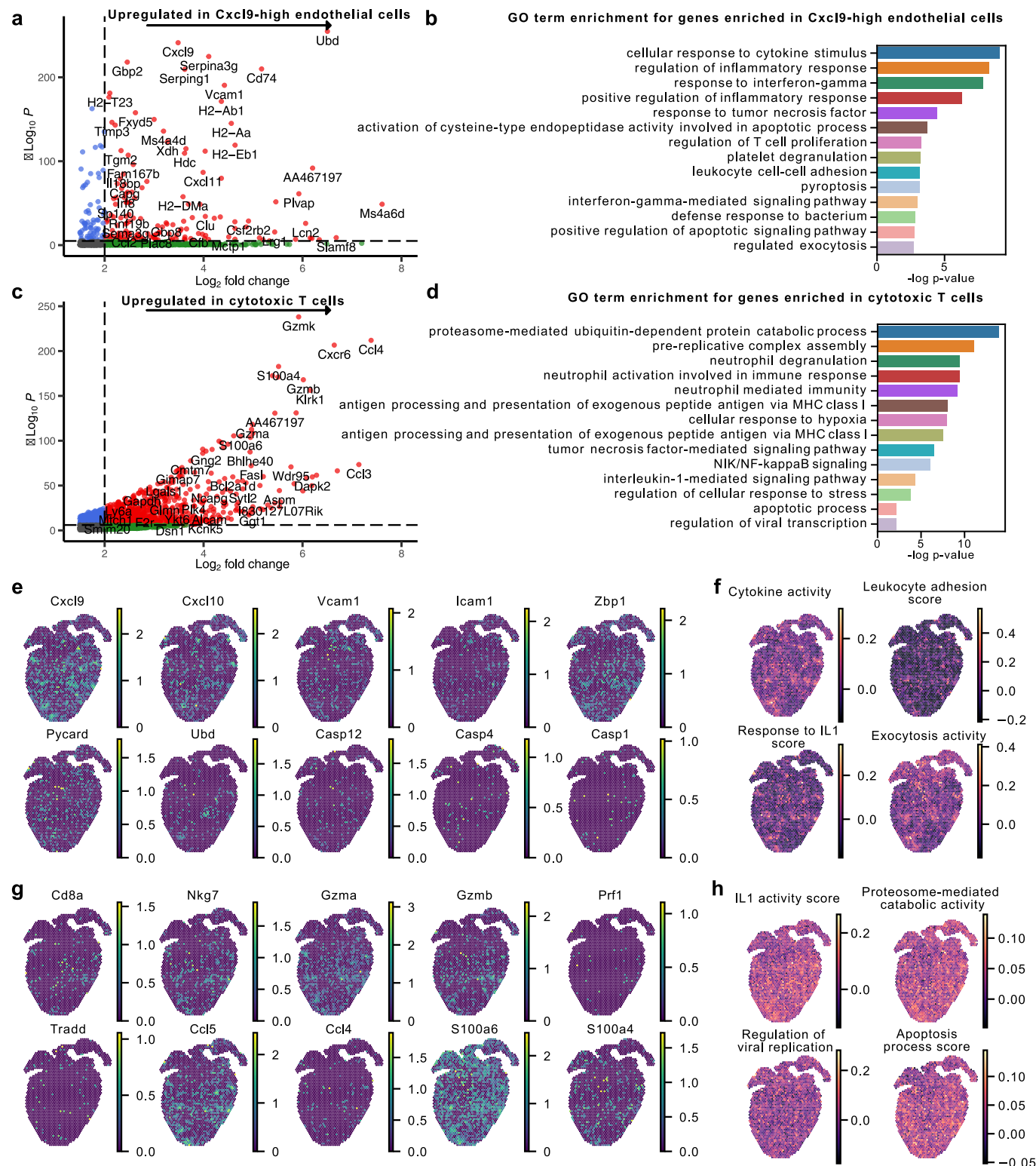
Extended Data Fig. 4 | Imaging-based characterization of spatial distribution of different cardiac cell types in infected cardiac tissue. **a)** Hematoxylin and Eosin (H&E) stained images of cardiac tissue sections from reovirus infected and mock infected mice at 7 dpi. **b)** Immunofluorescence staining of reovirus antigen in cardiac tissue sections from reovirus-infected and mock-infected hearts at 7 dpi. **c-d)** RNA FISH labeling of cell-type specific markers in reovirus-infected and mock-infected hearts at 7 dpi: macrophages (*Itgam* + *C1qa* +), dendritic cells

(*Itgam* + *C1qa* -), neutrophils (*S100a8*) and T cells (*Trbc2*). **e)** RNA FISH labeling of endothelial cell marker *Cdh5* and reovirus transcript (segment M3) in reovirus-infected and mock-infected hearts at 7 dpi. White arrows point at cell with reovirus transcripts. **b-e)** Representative images from 14 reovirus-infected (n = 7 males and n = 7 females) and six mock-infected (n = 3 males and n = 3 females) biological replicate mice.



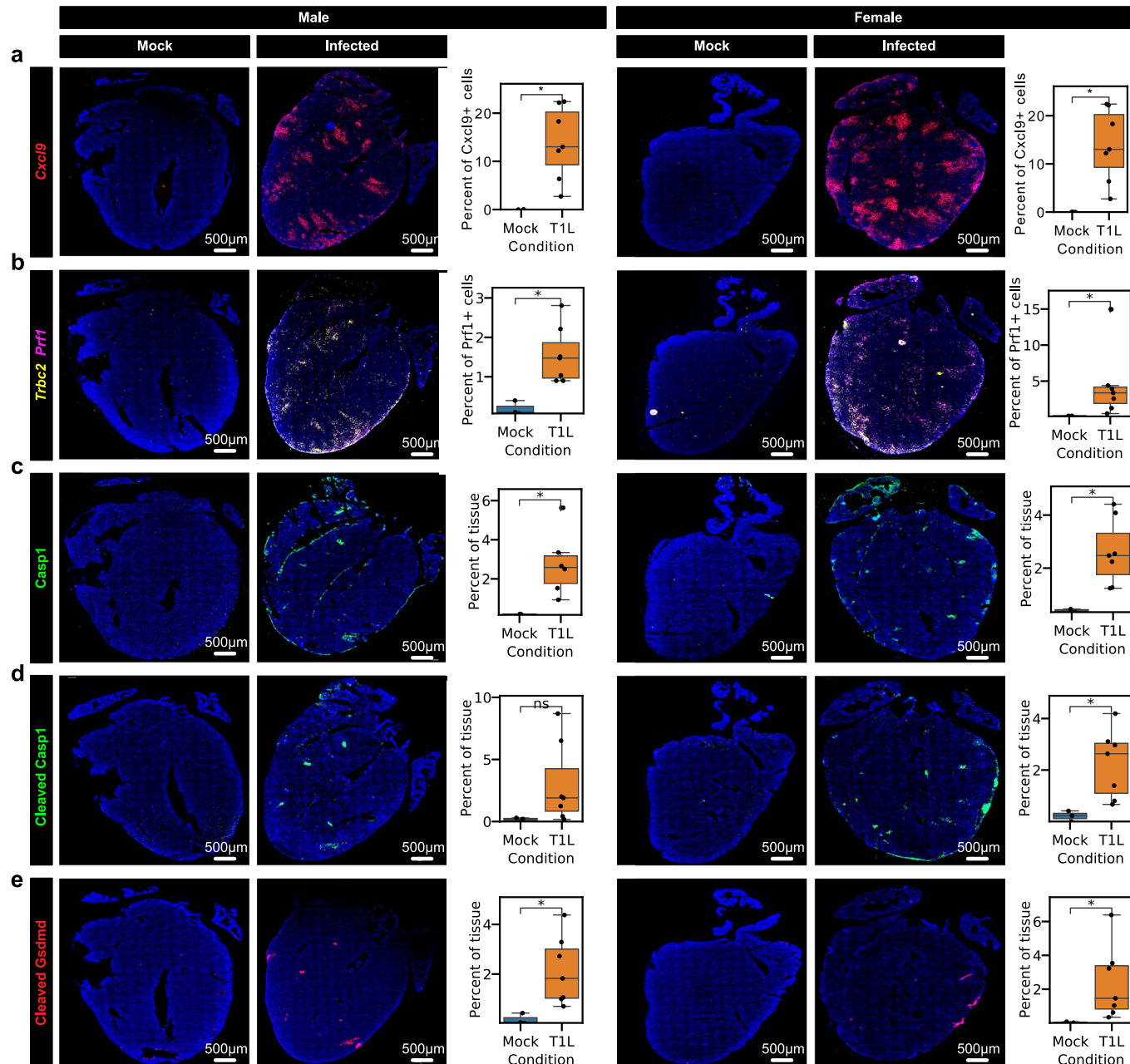
Extended Data Fig. 5 | Innate immune response across cell types in heart and ileum tissue from reovirus-infected neonatal mice. a) Volcano plot showing differentially expressed genes (two-sided Wilcoxon Rank-Sum test, $-\log_2$ fold change > 2.0 and p -value $< 10^{-4}$) for reovirus-infected cardiac cells as compared to mock at 4 dpi. Dotted lines show the thresholds for significantly enriched

genes (red). b) Top Gene Ontology (GO) terms for genes enriched in reovirus-infected cardiac cells as compared to mock at 4 dpi. **c)** Heatmap showing the expression of the 25 most upregulated genes in the reovirus-infected ileum as compared to mock at 1 dpi. **d)** Top GO terms for genes enriched in reovirus infected cells ileum as compared to mock-infected ileum at 1 dpi.



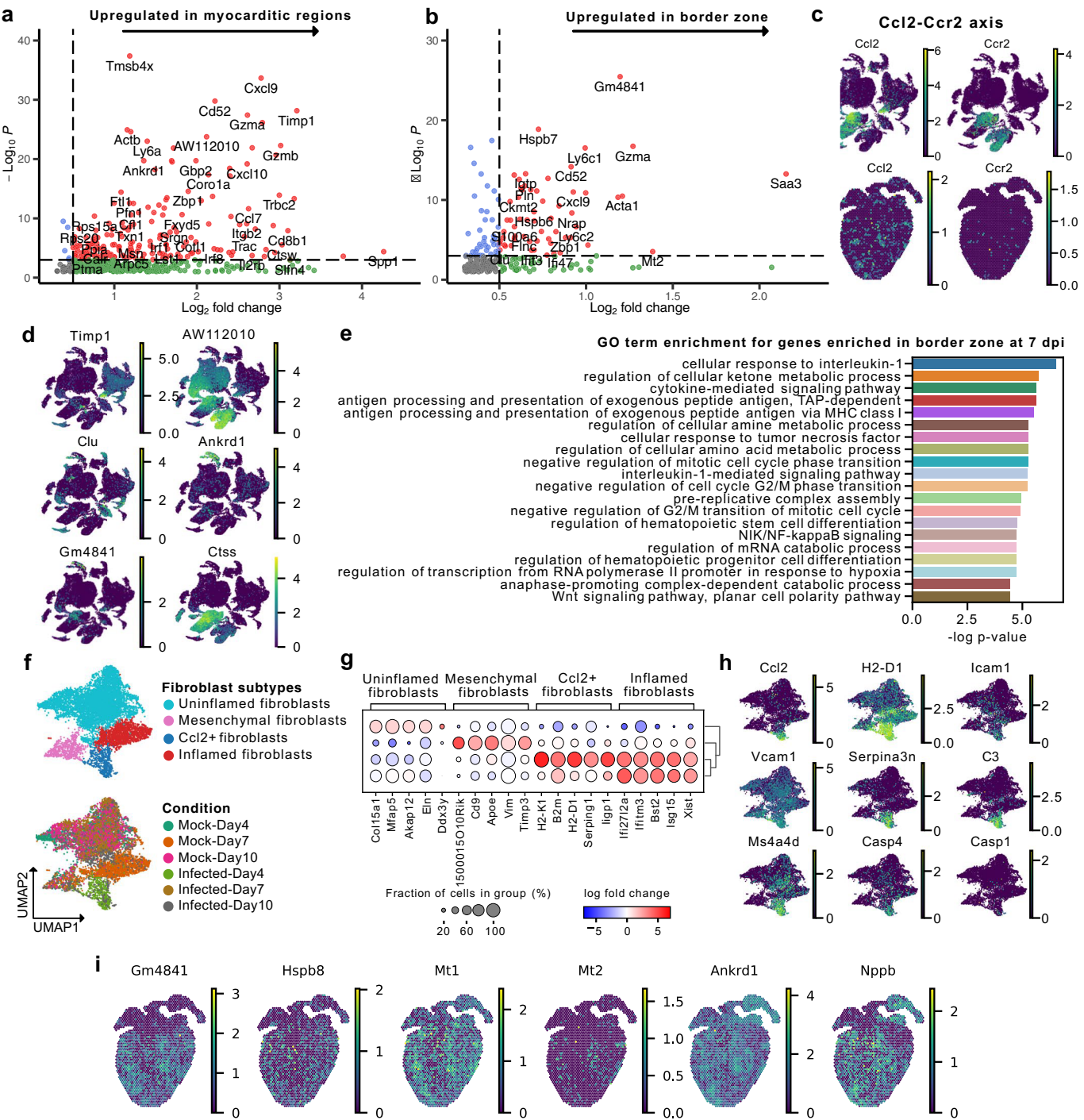
Extended Data Fig. 6 | Transcriptional gene signatures and programs for Cxcl9-high endothelial cells and cytotoxic T cells found within the myocarditic tissue. **a)** Volcano plot showing differentially expressed genes (two-sided Wilcoxon Rank-Sum test, $-\log_2$ fold change > 2.0 and p -value $< 10^{-4}$) upregulated in Cxcl9-high inflamed endothelial cells from heart at 7 dpi. Dotted lines show the thresholds for significantly enriched genes (red). **b)** Top Gene Ontology (GO) terms of interest enriched for genes upregulated in Cxcl9-high endothelial cells in myocarditic heart at 7 dpi. **c)** Volcano plot showing differentially expressed genes (two-sided Wilcoxon Rank-Sum test, $-\log_2$ fold change > 2.0 and p -value $< 10^{-4}$) upregulated in cytotoxic T cells at 7 and 10 dpi. Dotted lines show thresholds for significantly enriched genes (red). **d)** Top GO terms of interest enriched for genes upregulated in cytotoxic T cells in myocarditic hearts at 7 and 10 dpi. **e-h)** Spatial transcriptomics maps of cardiac tissue sections from reovirus-infected mice pups at 7 dpi showing: **e)** The expression of genes enriched in Cxcl9-high inflamed endothelial cells. **f)** Gene module scores for four GO terms of interest enriched in Cxcl9-high inflamed endothelial cells. **g)** The expression of genes enriched in cytotoxic T cells from myocarditic heart. **h)** Gene module scores calculated for four GO terms of interest enriched in cytotoxic T cells from myocarditic heart.

7 and 10 dpi. Dotted lines show thresholds for significantly enriched genes (red). **d)** Top GO terms of interest enriched for genes upregulated in cytotoxic T cells in myocarditic hearts at 7 and 10 dpi. **e-h)** Spatial transcriptomics maps of cardiac tissue sections from reovirus-infected mice pups at 7 dpi showing: **e)** The expression of genes enriched in Cxcl9-high inflamed endothelial cells. **f)** Gene module scores for four GO terms of interest enriched in Cxcl9-high inflamed endothelial cells. **g)** The expression of genes enriched in cytotoxic T cells from myocarditic heart. **h)** Gene module scores calculated for four GO terms of interest enriched in cytotoxic T cells from myocarditic heart.



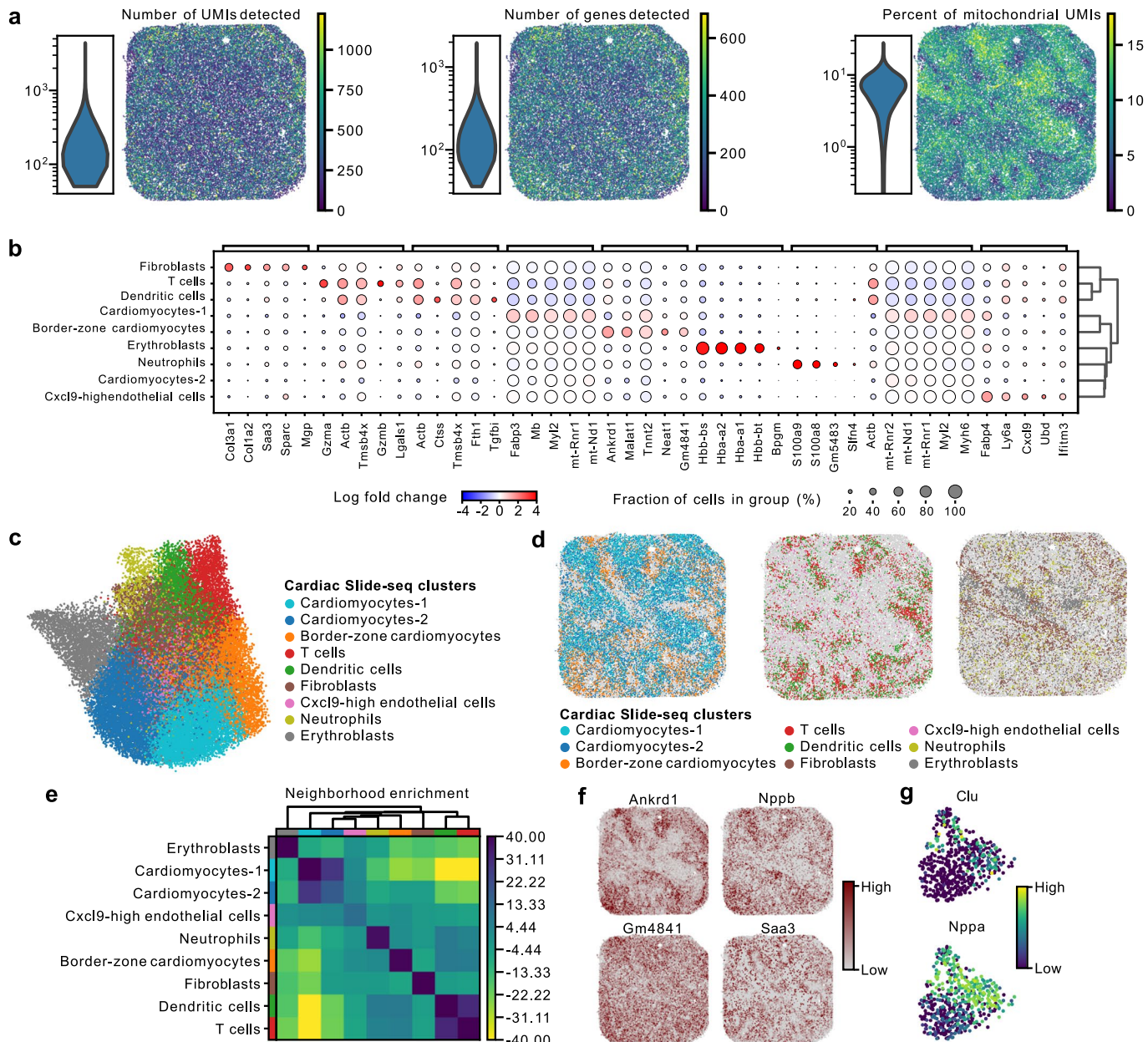
Extended Data Fig. 7 | Imaging-based characterization of *Cxcl9*-high endothelial cells, cytotoxic T cells, and pyroptosis in myocarditic tissue. **a)** RNA FISH labelling of *Cxcl9* transcripts in *Cdh5*+ endothelial cells in reovirus-infected and mock infected hearts at 7 dpi. **b)** RNA FISH labelling of *Prf1* transcripts in *Trbc2*+ T cells in reovirus-infected and mock-infected hearts, confirming the recruitment of cytotoxic T cells in myocarditic tissue (bottom row). **c-e)** Immunostaining of protein markers for pyroptosis activity: **c)** Casp1 protein (Pro-caspase1 and cleaved Caspase1) **d)** Cleaved Caspase1 protein (only Casp1 p20 subunit) and **e)** Cleaved Gasdermin D (*Gsdmd* N terminus fragment) in reovirus-infected and mock-infected hearts at 7 dpi. **a-e)** Representative

images from 14 reovirus-infected mice (n = 7 males and n = 7 females) and six mock-infected mice (n = 3 males and n = 3 females). Immunofluorescence signal from reovirus-infected hearts was compared to mock-infected hearts using two-sided Wilcoxon statistical test. Boxes in the boxplots indicates 25th and 75th percentile, the band in the box indicated the median and whiskers extend to $1.5 \times$ Interquartile Range (IQR) of the hinge. Outliers (beyond $1.5 \times$ IQR) are plotted individually (n = 14 biologically independent reovirus infected tissues and n = 6 biologically independent mock-infected tissues). p-value annotation legend: ns: p $\geq 1.00e + 00$, *: $1.00e - 02 < p \leq 5.00e - 02$, **: $1.00e - 03 < p \leq 1.00e - 02$, ***: $1.00e - 04 < p \leq 1.00e - 03$, ****: p $\leq 1.00e - 04$.



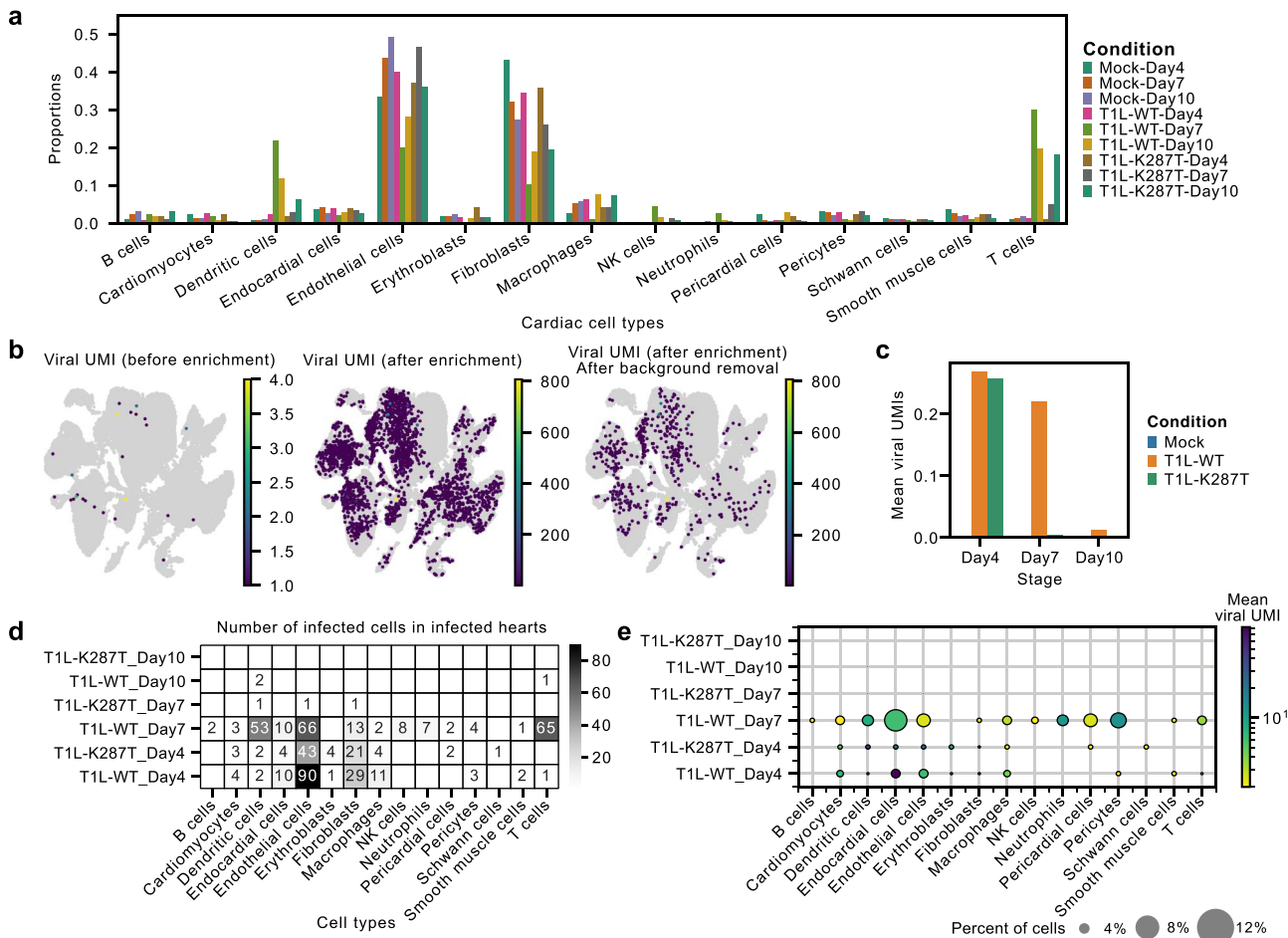
Extended Data Fig. 8 | Cell-type-specific gene expression in myocarditic tissue and characterization of inflamed fibroblast phenotype found within the myocarditic tissue. **a**) Volcano plot showing differentially expressed genes (two-sided Wilcoxon Rank-Sum test, $-\log_2$ fold change > 0.5 and p -value $< 10^{-2}$) upregulated in myocarditic regions in heart at 7 dpi as defined by unsupervised clustering on spatial transcriptomes. Dotted lines show the thresholds for significantly enriched genes (red). **b**) Volcano plot showing differentially expressed genes (two-sided Wilcoxon Rank-Sum test, $-\log_2$ fold change > 0.5 and p -value $< 10^{-2}$) upregulated in the border zone of the infected heart at 7 dpi, as defined by unsupervised clustering on spatial transcriptomes. Dotted lines represent thresholds for significantly enriched genes (red). **c**) UMAP plot for heart scRNA-seq cells and spatial transcriptomic maps for reovirus-infected heart at 7 dpi showing the expression of *Ccl2* ligand and *Ccr2* receptor. **d**) scRNA-seq UMAP plots showing the expression of six genes of interest enriched in myocarditic regions and the border zone. **e**) Top GO terms of interest for genes upregulated in *Cxcl9*-high endothelial cells in myocarditic heart at 7 dpi. **f**) UMAP plot of 9,192 fibroblast cell transcriptomes from mock-infected and reovirus-infected hearts at 4, 7, and 10 dpi colored by fibroblast cell subtypes (phenotypes) (top) and condition (bottom). **g**) Heatmap showing top-five differentially expressed genes (two-sided Wilcoxon test, \log_2 fold-change > 1.0 and p -value < 0.01) for fibroblast cell subtypes. **h**) UMAP plot showing the expression of genes upregulated in *Ccl2*+ fibroblast cells. **i**) Spatial transcriptomic maps for myocarditic heart at 7 dpi showing the expression of six myocyte-specific genes upregulated in the border zone.

dpi showing the expression of *Ccl2* ligand and *Ccr2* receptor. **d**) scRNA-seq UMAP plots showing the expression of six genes of interest enriched in myocarditic regions and the border zone. **e**) Top GO terms of interest for genes upregulated in *Cxcl9*-high endothelial cells in myocarditic heart at 7 dpi. **f**) UMAP plot of 9,192 fibroblast cell transcriptomes from mock-infected and reovirus-infected hearts at 4, 7, and 10 dpi colored by fibroblast cell subtypes (phenotypes) (top) and condition (bottom). **g**) Heatmap showing top-five differentially expressed genes (two-sided Wilcoxon test, \log_2 fold-change > 1.0 and p -value < 0.01) for fibroblast cell subtypes. **h**) UMAP plot showing the expression of genes upregulated in *Ccl2*+ fibroblast cells. **i**) Spatial transcriptomic maps for myocarditic heart at 7 dpi showing the expression of six myocyte-specific genes upregulated in the border zone.



Extended Data Fig. 9 | High-resolution slide-seq spatial transcriptomics of cardiac tissue from reovirus-infected neonatal mice. **a)** Number of unique UMIs detected per cell (left), number of unique genes detected per cell (center), and percentage of mitochondrial transcripts (right) in slide-seq datasets from reovirus infected heart at 7 dpi. **b)** Heatmap showing top-five differentially expressed genes (two-sided Wilcoxon test, \log_2 fold-change > 1.0 and p -value < 0.01) for slide-seq spatial transcriptomics clusters. **c)** UMAP plot of $> 40,000$ slide-seq spatial transcriptomes from reovirus-infected heart at 7 dpi, clustered by gene expression and colored by putative cardiac cell types

based on differential gene expression and marker analysis. **d)** Slide-seq spatial transcriptomics maps showing three slide-seq clusters at a time. **e)** Heatmap of permutation test scores for neighborhood enrichment of slide-seq clusters. Enrichment scores reflect enrichment of spatial proximity of slide-seq clusters. **f)** Slide-seq spatial transcriptomics maps showing the expression of border-zone cardiomyocyte specific genes. **g)** UMAP plot showing the scRNAseq expression of cardiomyocyte-specific genes which are upregulated in border-zone myocytes in the slide-seq data.



Extended Data Fig. 10 | Differences in cell type composition and viral tropism between scRNA-seq cells from reovirus WT and K287T mutant-infected neonatal mice. **a)** Bar plot showing the cell type composition changes in scRNA-seq datasets from reovirus WT and K287T mutant-infected cardiac tissue. **b)** scRNA-seq UMAP plots showing total viral UMI counts per cell before xGen enrichment, after xGen viral transcript enrichment, and after removal of

background signal on heart samples. **c)** Bar plot showing mean viral transcript count (UMIs) across stages for reovirus WT- and K287T mutant-infected hearts. **d)** Heatmaps showing counts of infected cells of different cardiac cell types across reovirus WT and K287T mutant-infected heart samples. **e)** Dot plot showing the percentage of cells with non-zero viral transcripts and the mean viral transcript counts (UMIs) across cell types.

Reporting Summary

Nature Portfolio wishes to improve the reproducibility of the work that we publish. This form provides structure for consistency and transparency in reporting. For further information on Nature Portfolio policies, see our [Editorial Policies](#) and the [Editorial Policy Checklist](#).

Statistics

For all statistical analyses, confirm that the following items are present in the figure legend, table legend, main text, or Methods section.

n/a Confirmed

- The exact sample size (n) for each experimental group/condition, given as a discrete number and unit of measurement
- A statement on whether measurements were taken from distinct samples or whether the same sample was measured repeatedly
- The statistical test(s) used AND whether they are one- or two-sided
Only common tests should be described solely by name; describe more complex techniques in the Methods section.
- A description of all covariates tested
- A description of any assumptions or corrections, such as tests of normality and adjustment for multiple comparisons
- A full description of the statistical parameters including central tendency (e.g. means) or other basic estimates (e.g. regression coefficient) AND variation (e.g. standard deviation) or associated estimates of uncertainty (e.g. confidence intervals)
- For null hypothesis testing, the test statistic (e.g. F , t , r) with confidence intervals, effect sizes, degrees of freedom and P value noted
Give P values as exact values whenever suitable.
- For Bayesian analysis, information on the choice of priors and Markov chain Monte Carlo settings
- For hierarchical and complex designs, identification of the appropriate level for tests and full reporting of outcomes
- Estimates of effect sizes (e.g. Cohen's d , Pearson's r), indicating how they were calculated

Our web collection on [statistics for biologists](#) contains articles on many of the points above.

Software and code

Policy information about [availability of computer code](#)

Data collection

No software was used for data collection.

Data analysis

scRNASeq and Visium spatial transcriptomics data analysis was performed using CellRanger Single Cell Software Suite (6.0.0), Loupe Browser 4.0.0, SpaceRanger Spatial RNASeq software Suite (1.0.0), Scanpy (v1.8.1 & v1.9.1), scvi-tools (v0.16.4), and gseapy (v0.10.4), Squidpy (v1.2.2), Cell2location (v0.1), seaborn (v0.11.1), and matplotlib (v3.3.4). Spatial RNASeq tissue images were stitched using Fiji ImageJ software. FISH and immunostaining images were analyzed using Zen 3.1 (blue edition) and Fiji ImageJ (v1.52p) software.

Scripts to reproduce the analysis presented in this study have been deposited on GitHub (https://github.com/madhavmantri/reovirus_induced_myocarditis).

For manuscripts utilizing custom algorithms or software that are central to the research but not yet described in published literature, software must be made available to editors and reviewers. We strongly encourage code deposition in a community repository (e.g. GitHub). See the Nature Portfolio [guidelines for submitting code & software](#) for further information.

Data

Policy information about [availability of data](#)

All manuscripts must include a [data availability statement](#). This statement should provide the following information, where applicable:

- Accession codes, unique identifiers, or web links for publicly available datasets
- A description of any restrictions on data availability
- For clinical datasets or third party data, please ensure that the statement adheres to our [policy](#)

The authors declare that all sequencing data supporting the findings of this study have been deposited in NCBI's Gene Expression Omnibus (GEO)57 with GEO series

accession number GSE189636. Sequencing data for high-resolution Slide-seq spatial transcriptomics has been deposited in NCBI's GEO with series accession number GSE211096. Raw and processed H&E-stained tissue images and tissue-spot alignment files matched to spatial transcriptomics datasets have been made publicly available on figshare with identifier <https://doi.org/10.6084/m9.figshare.c.572637258>. All other data supporting the findings in this study are included in the main article and associated files.

Mus musculus genome and gene annotations (assembly: GRCh38) were downloaded from the Ensembl genome browser, and reovirus strain type-1 Lang genome and gene annotations were downloaded and compiled from the NCBI browser. We have shared reovirus genome sequence and annotation files on figshare with the identifier <https://doi.org/10.6084/m9.figshare.c.5726372>.

Field-specific reporting

Please select the one below that is the best fit for your research. If you are not sure, read the appropriate sections before making your selection.

Life sciences Behavioural & social sciences Ecological, evolutionary & environmental sciences

For a reference copy of the document with all sections, see nature.com/documents/nr-reporting-summary-flat.pdf

Life sciences study design

All studies must disclose on these points even when the disclosure is negative.

Sample size	No sample size calculation was performed for this study. Due to the high cost of sequencing assays, n=1 mouse was used to collect tissue for each experiment condition in scRNAseq and spatial transcriptomics experiments. To validate the findings from the analysis of sequencing data, RNA FISH and immunostaining assays were performed on n=14 biologically-independent reovirus-infected mice and n=6 biologically-independent mock-infected mice. RNA FISH and immunostaining assays confirmed the results with statistical significance.
Data exclusions	No data were excluded from the analysis.
Replication	Extensive histology, multiplexed RNA fluorescence in-situ hybridization (FISH), and immunostaining assays were used to validate all findings on multiple pairs of male and female tissues from independent litters. One pair of mock tissues from male and female mice, two pairs of male and female tissues from Reovirus Type-1-Lang infected mice, and another two pairs of male and female tissues from Reovirus K287T-infected mice were used for validation experiments.
Randomization	The mice used to collect ileum and heart tissues for scRNAseq and spatial transcriptomics experiments were randomly selected from the litters at the respective experiment stages. Ileum and hearts were assayed from the same animal at day 4 post-infection time point. Heart tissues at day 7 post-infection were selected for the presence of scarred tissue before performing scRNAseq and spatial transcriptomics experiments.
Blinding	Blinding was not possible in this study as visible inspection of the hearts from neonatal mice was used to confirm the presence of scarred tissue/ myocarditic lesions.

Reporting for specific materials, systems and methods

We require information from authors about some types of materials, experimental systems and methods used in many studies. Here, indicate whether each material, system or method listed is relevant to your study. If you are not sure if a list item applies to your research, read the appropriate section before selecting a response.

Materials & experimental systems

n/a	Involved in the study
<input type="checkbox"/>	<input checked="" type="checkbox"/> Antibodies
<input checked="" type="checkbox"/>	<input type="checkbox"/> Eukaryotic cell lines
<input checked="" type="checkbox"/>	<input type="checkbox"/> Palaeontology and archaeology
<input type="checkbox"/>	<input checked="" type="checkbox"/> Animals and other organisms
<input checked="" type="checkbox"/>	<input type="checkbox"/> Human research participants
<input checked="" type="checkbox"/>	<input type="checkbox"/> Clinical data
<input checked="" type="checkbox"/>	<input type="checkbox"/> Dual use research of concern

Methods

n/a	Involved in the study
<input type="checkbox"/>	<input checked="" type="checkbox"/> ChIP-seq
<input checked="" type="checkbox"/>	<input type="checkbox"/> Flow cytometry
<input checked="" type="checkbox"/>	<input type="checkbox"/> MRI-based neuroimaging

Antibodies

Antibodies used

1. Rabbit anti-Reovirus VM1:VM6 polyclonal Sera (Supplier: Custom made, Dilution: 1:30000),
2. Rat anti-Casp1 monoclonal antibody (Supplier: Invitrogen, Catalog number: #14-9832-82, Clone: 5B10 , Dilution: 1:200).
3. Donkey anti-rabbit Alexa-488 (Supplier: Jackson Immuno Research, Catalog number: 711-545-152, Dilution: 1:500)
4. Donkey anti-rabbit Alexa647 (Supplier: Jackson Immuno Research, Catalog number: 711-605-152, Dilution: 1:500)
5. Donkey anti-rat Alexa-647 (Supplier: Abcam, Catalog number: ab150155, Dilution: 1:500).

Validation

1. Rabbit anti-Reovirus VM1:VM6 polyclonal Sera (Supplier: Custom made, Dilution: 1:30000)
 Validation: This is custom made reovirus polyclonal sera purchased from Cocalico Biologicals in the 90's. New Zealand white rabbits were inoculated with reovirus T1L (sera called VM1) or reovirus T3D (sera called VM6) and serum was collected at different intervals. These sera were combined 1:1, pre-adsorb on L929 cells, and was used and characterized by Barton et al. in 2001. Citation: Barton, E.S., Connolly, J.L., Forrest, J.C., Chappell, J.D. & Dermody, T.S. Utilization of sialic acid as a coreceptor enhances reovirus attachment by multistep adhesion strengthening. *J Biol Chem* 276, 2200-11 (2001).
2. Rat anti-Casp1 monoclonal antibody (Supplier: Invitrogen, Catalog number: #14-9832-82, Clone: 5B10, Dilution: 1:200).
 Validation: According to manufacturer's website, the antibody has been tested by western blot analysis of lysates prepared from the J774 cell line validated to be reactive on mouse samples for western blot and immunohistochemistry/IF and has been cited by 13 publications. This Antibody was also verified by Cell treatment to ensure that the antibody binds to the antigen stated. The antibody has been cited by 27 publication on CiteAb.com.
3. Rabbit anti-cleaved Caspase1 (Asp297) (Supplier: Cell Signaling Technology, Catalog number: #4199T, Dilution: 1:200).
 Validation: According to the manufacturer's website, the antibody has been used for western blot analysis of cell extracts from the cells or media from mouse bone marrow derived macrophages (mBMDM), untreated (-) or treated with Lipopolysaccharides (LPS), followed by Nigericin (15 µM, 45 min) (+) to show that cleaved Caspase-1 (Asp296) (E2G2I) Rabbit mAb recognizes endogenous levels of caspase-1 protein only when cleaved at Asp296. The antibody has been cited by 76 publications on CiteAb.com
4. Rabbit anti-cleaved Gasdermin D (Asp275) (Supplier: Cell Signaling Technology, Catalog number: #36425S, Dilution: 1:200).
 Validation: According to the manufacturer's website, the antibody has been used for western blot analysis of extracts from mouse bone marrow derived macrophages (mBMDM), untreated (-) or treated with Lipopolysaccharides (LPS) #14011 (50 ng/ml, 4 hr; +) followed by Nigericin (sodium salt) #66419 (15 µM, indicated times; +), using Cleaved Gasdermin D (Asp276) (E3E3P) Rabbit mAb (upper) to show that Cleaved Gasdermin D (Asp276) (E3E3P) Rabbit mAb recognizes endogenous levels of the amino fragment of mouse Gasdermin D protein only when cleaved at Asp276. The antibody has been cited by 8 publications on CiteAb.com.

Animals and other organisms

Policy information about [studies involving animals; ARRIVE guidelines](#) recommended for reporting animal research

Laboratory animals

All animal work was conducted ethically, conforming to the U.S. Public Health Service policy, and was approved by the Institutional Animal Care and Use Committee at Cornell University (IACUC Number 2019-0129). Confirmed pregnant female C57BL/6J mice were ordered from Jackson Laboratories to be delivered at embryonic stage E14.5. Litters weighing 3 gram/pup were gavaged per os with reovirus type 1 Lang (T1L): wildtype/K287T mutant or with 1x PBS containing green food color for infection and mock groups. The strain, sex, and age of every animal used in the study are as follows (sex of the neonatal animals was determined by expression of Xist gene from the sequencing data):

Heart_10x_scRNAseq_Mock_Day4: Strain/Substrain=C57BL/6J; Age=8 days; Sex=Male
 Heart_10x_scRNAseq_T1L_WT_Day4: Strain/Substrain=C57BL/6J; Age=8 days; Sex=Female
 Heart_10x_scRNAseq_T1L-K287T_Day4: Strain/Substrain=C57BL/6J; Age=8 days; Sex=Male
 Heart_10x_scRNAseq_Mock_Day7: Strain/Substrain=C57BL/6J; Age=11 days ; Sex=Male
 Heart_10x_scRNAseq_T1L_WT_Day7: Strain/Substrain=C57BL/6J; Age=11 days ; Sex=Female
 Heart_10x_scRNAseq_T1L-K287T_Day7: Strain/Substrain=C57BL/6J; Age=11 days ; Sex=Female
 Heart_10x_scRNAseq_Mock_Day10: Strain/Substrain=C57BL/6J; Age=14 days; Sex=Female
 Heart_10x_scRNAseq_T1L_WT_Day10: Strain/Substrain=C57BL/6J; Age=14 days; Sex=Female
 Heart_10x_scRNAseq_T1L-K287T_Day10: Strain/Substrain=C57BL/6J; Age=14 days; Sex=Female
 Heart_Visium_ST_Mock_Day4: Strain/Substrain=C57BL/6J; Age=8 days; Sex=Female
 Heart_Visium_ST_T1L-WT_Day4: Strain/Substrain=C57BL/6J; Age=8 days; Sex=Female
 Heart_Visium_ST_Mock_Day7: Strain/Substrain=C57BL/6J; Age=11 days ; Sex=Male
 Heart_Visium_ST_T1L-WT_Day7: Strain/Substrain=C57BL/6J; Age=11 days ; Sex=Male
 Heart_SlideSeq_ST_T1L-WT_Day7: Strain/Substrain=C57BL/6J; Age=11 days ; Sex=Female
 Ileum_10x_scRNAseq_Mock_Day1: Strain/Substrain=C57BL/6J; Age=5 days; Sex=Male
 Ileum_10x_scRNAseq_T1L_WT_Day1: Strain/Substrain=C57BL/6J; Age=5 days; Sex=Female
 Ileum_10x_scRNAseq_Mock_Day4: Strain/Substrain=C57BL/6J; Age=8 days; Sex=Male
 Ileum_10x_scRNAseq_T1L_WT_Day4: Strain/Substrain=C57BL/6J; Age=8 days; Sex=Female
 Ileum_Visium_ST_Mock_Day1: Strain/Substrain=C57BL/6J; Age=5 days; Sex=Female
 Ileum_Visium_ST_T1L-WT_Day1: Strain/Substrain=C57BL/6J; Age=5 days; Sex=Female
 Ileum_Visium_ST_Mock_Day4: Strain/Substrain=C57BL/6J; Age=8 days; Sex=Female
 Ileum_Visium_ST_T1L-WT_Day4: Strain/Substrain=C57BL/6J; Age=8 days; Sex=Male

Wild animals

The study did not involve any wild animal.

Field-collected samples

The study did not involve samples collected from the field.

Ethics oversight

All animal work was conducted ethically, conforming to the U.S. Public Health Service policy, and was approved by the Institutional Animal Care and Use Committee at Cornell University (IACUC Number 2019-0129).

Note that full information on the approval of the study protocol must also be provided in the manuscript.